Knocking out non-muscle myosin II in retinal ganglion cells promotes long-distance optic nerve regeneration

Xue-Wei Wang[1, †], Shu-Guang Yang[1, †], Chi Zhang[1, †], Jin-Jin Ma[3], Yingchi Zhang[1], Bin-Bin Yang[1], Yi-Lan Weng[5], Guo-Li Ming[6], Anish R. Kosanam[1], Saijilafu[3, 4, *], and Feng-Quan Zhou[1, 2, *]

[1]Department of Orthopaedic Surgery, The Johns Hopkins University School of Medicine, Baltimore, MD 21287

[2]The Solomon H. Snyder Department of Neuroscience, The Johns Hopkins University School of Medicine, Baltimore, MD 21287

[3]Orthopaedic Institute, Medical College, Soochow University, Suzhou, Jiangsu, China

[4]Department of Orthopaedic Surgery, the First Affiliated Hospital, Soochow University, Suzhou, China

[5]Center for Neuroregeneration, Department of Neurosurgery, Houston Methodist Research Institute, Houston, TX 77030

[6]Department of Neuroscience, Perelman School of Medicine, University of Pennsylvania, Philadelphia, PA 19104

[†]These authors contributed equally to this study

*Correspondence to:

Feng-Quan Zhou, Ph.D., Room 291, The John G. Rangos Sr. Building, 855 North Wolfe Street, Baltimore, MD 21287, Email: fzhou4@jhmi.edu

Saijilafu, Ph.D. Orthopaedic Institute, Medical College, Soochow University, Suzhou, Jiangsu, China Email: saijilafu@suda.edu.cn

Abstract

In addition to altered gene expression, pathological cytoskeletal dynamics in the axon are another key intrinsic barrier for axon regeneration in the central nervous system (CNS). Here we showed that knocking out myosin IIA/B in retinal ganglion cells alone either before or after optic nerve crush induced marked and sustained optic nerve regeneration. Combined Lin28 overexpression and myosin IIA/B knockout led to synergistic promoting effect and long-distance axon regeneration. Immunostaining, RNA-seq and western blot analyses revealed that myosin II deletion did not affect known axon regeneration signaling pathways or the expression of regeneration associated genes. Instead, it abolished the retraction bulb formation and significantly enhanced the axon extension efficiency. The study provided clear evidence that directly targeting neuronal cytoskeleton was sufficient to induce strong CNS axon regeneration, and combining gene expression in the soma and modified cytoskeletal dynamics in the axon was a promising approach for long-distance CNS axon regeneration.

Keywords

Axon regeneration, optic nerve regeneration, non-muscle myosin II, Lin28, growth cone, cytoskeleton

Introduction

Axon regeneration in the mammalian central nervous system (CNS) has been a long standing and highly challenging issue in the biomedical research field. The current consensus is that there are two major reasons that neurons in the mature mammalian CNS do not regenerate their axons after injury. One is the hostile environment created by inhibitors in the scar tissues and degenerating myelin, and the other is the diminished intrinsic neural regeneration ability of mature CNS neurons (*1, 2*). Therefore, the widely accepted view is that combination strategies that target both intrinsic growth ability and inhibitory environment are likely the best option for successful CNS axon regeneration and function recovery. Early studies (*3-6*) using peripheral nerve graft transplants have shown that some mature CNS neurons, such as spinal cord neurons and retinal ganglion cells (RGCs), could regenerate their axons into the permissive nerve grafts, indicating clearly that these neurons still retain limited intrinsic regeneration ability. However, to date, many studies targeting selected inhibitory molecules resulted in no or very modest CNS regeneration (*7, 8*). A likely reason is that there are multiple classes of inhibitory molecules, potentially including unidentified ones, which inhibit axon regeneration via distinct cellular and molecular mechanisms. Thus, targeting a few inhibitory signals while leaving the others intact may not result in a permissive environment similar to that in the peripheral nerve grafts.

In contrast, studies targeting the intrinsic axon growth ability have produced very promising results. In the optic nerve regeneration model, for example, Pten, Socs3, Klf4 loss of function, and Lin28 gain of function all achieved strong optic nerve regeneration (*9-13*). However, tissue clearing and 3D imaging studies have revealed that many of the regenerating RGC axons make U-turns in the optic nerve, at the optic chiasm, or make wrong guidance decisions after the chiasm (*14, 15*). In the corticospinal tract (CST) regeneration model, although modulation of the intrinsic regeneration ability substantially enhanced axon regeneration, most regenerating axons still cannot pass the lesion site, likely due to the effects of inhibitory

62 molecules at the injury site, especially glial scar-based inhibitors. For instance, Pten deletion has been
63 shown to induce by far the strongest promoting effect on CST axon regeneration (*16*). However, the most
64 robust promoting effect can only be achieved in young mice (< 1 month). A recent study (*17*) showed that
65 Pten deletion-induced regeneration of CST axons beyond the injury site was greatly diminished in aged
66 mice. Specifically, in 12-18-month-old mice, Pten deletion led to little, if any, CST regeneration beyond
67 the injury site. One likely reason for the diminished effect in older animals was the increased response to
68 the inhibitory CNS environment. Thus, developing a successful approach for stimulating regeneration of
69 injured CST remains a challenge, especially in older animals. Together, a new strategy is needed to enable
70 neurons with increased intrinsic axon growth ability to grow axons in the inhibitory environment more
71 efficiently with fewer U-turns and unnecessary branching, and can cross the inhibitory boundary more
72 efficiently.

73 Neuronal cytoskeleton is not only the major machinery that drives axon growth (*18-20*), but also
74 the converging targets of most, if not all, inhibitory signaling pathways (*18, 20*). In other words, by directly
75 manipulating growth cone cytoskeletal motility it is possible to interfere with how the growth cones
76 respond to multiple inhibitory signals, regardless if these signals are from different inhibitors or
77 downstream pathways. Indeed, our previous study (*21*) showed that knocking down or pharmacologically
78 inhibiting non-muscle myosin IIA/B could allow regenerating sensory axons to grow straight, make less
79 branches, and completely ignore chondroitin sulfate proteoglycans (CSPGs) and myelin-based inhibitors.
80 The effects were much stronger than that of Rho kinase inhibitor. Mechanistically, inhibition of myosin
81 IIA/B resulted in loss of lamellipodia and actin arc, which led to significantly enhanced microtubule
82 protrusion towards the leading edge of the growth cone. As a result, the axon growth rate over permissive
83 substrate was greatly accelerated, and halted axon growth over inhibitory substrates was immediately
84 restarted. Here we examined if knocking out non-muscle myosin IIA/B in RGCs could promote optic

85 nerve regeneration in vivo. The results showed that deleting myosin IIA/B alone was sufficient to induce
86 robust and sustained optic nerve regeneration. Moreover, combination of myosin IIA/B knockout and
87 Lin28 overexpression, which enhances the intrinsic axon regeneration ability of RGCs (*12*), led to
88 synergistic promoting effect and long-distance optic nerve regeneration. Importantly, the promoting effect
89 was independent of well-known signaling mediators of optic nerve regeneration, such as increased mTOR
90 activity and GSK3β inactivation (*2*). RNA-seq and western blot analyses comparing wild type and myosin
91 IIA/B knockout neurons showed no significant difference in the expression of known regeneration
92 associated genes, indicating local effects in the axons. In support, detailed analyses of growth cone
93 morphologies and axon trajectories revealed that myosin II deletion almost abolished the formation of
94 retraction bulbs, a hallmark of failed axon regeneration, and significantly enhanced the axon extension
95 efficiency in the optic nerve. Furthermore, knocking out myosin IIA/B after optic nerve crush similarly
96 enhanced optic nerve regeneration, indicating potential translational application. Collectively, our study
97 demonstrated clearly that manipulation of neuronal cytoskeleton alone was sufficient to promote
98 significant CNS axon regeneration in vivo. The study also provided strong evidence that combining
99 enhanced intrinsic regeneration ability in the neuronal soma with local manipulation of axonal
100 cytoskeleton was a promising approach to induce long-distance CNS axon regeneration in vivo.
101

102 **Results**

103 **Double knockout of non-muscle myosin IIA/B in RGCs led to significant and sustained optic nerve**
104 **regeneration in vivo**

105 Non-muscle myosin II consists of two essential light chains, two regulatory light chains, and a
106 myosin II heavy chain (MHC). There are three different isoforms of MHCs in mammalian cells, IIA, IIB,
107 and IIC, encoded by *Myh 9*,*10*, and *14* genes, respectively. Myosin IIA and IIB with MHC IIA/B (myosin
108 IIA/B) are the major isoforms in neurons (*21*). In nerve growth cones, both myosin IIA/B are localized
109 near the transition zone, where microtubules and actin filaments interact (*21*). Our previous study (*21*) has
110 shown that pharmacological inhibition or double knockdown of myosin IIA/B in developing or
111 regenerating sensory neurons drastically promoted sensory axon growth over two major inhibitory
112 substrates, myelin extracts or CSPGs. Here we tested if myosin IIA/B loss of function could also induce
113 axon regeneration in RGCs after optic nerve injury. To knock out both myosin IIA/B in RGCs, we crossed
114 *Myh9*$^{f/f}$ and *Myh10*$^{f/f}$ mice to generate *Myh9*$^{f/f}$*: Myh10*$^{f/f}$ mice (hereafter *myosin IIA/B*$^{f/f}$), and injected
115 AAV2-Cre into the vitreous humors of these mice. Wild type mice injected with AAV2-Cre were used in
116 the control group. To examine viral vector infection rate, immunostaining of Cre recombinase in whole-
117 mount retina was performed two weeks after the injection. The results showed that the infection rate in
118 RGCs was about 90% (Fig. S1A, C). Immunostaining of retinal sections also showed a nice colocalization
119 of Cre staining with Tuj1-positive RGCs (Fig. S1B). We also injected AAV2-Cre into tdTomato reporter
120 mice to examine the efficiency of Cre-mediated gene recombination. Strong expression of tdTomato in
121 RGCs was observed two weeks after AAV2-Cre injection (Fig. S2A, B), indicating successful gene
122 recombination. Lastly, we examined if myosin IIA/B were indeed deleted in RGCs after AAV2-Cre
123 injection. By western blot analysis of the whole retina tissue, we found that the protein level of myosin
124 IIA was markedly reduced (Fig. S3A). Immunostaining of retinal sections with anti-myosin IIB antibody

125 showed significantly reduced level of myosin IIB in RGCs (Fig. S3B, C). Together, these results
126 demonstrated clearly that myosin IIA/B were successfully deleted in RGCs.

127 To determine how myosin IIA/B double knockout (dKO) in RGCs affected optic nerve
128 regeneration, we performed optic nerve crush (ONC) 2 weeks after the viral injection. We first assessed
129 optic nerve regeneration 2 weeks after the ONC. The regenerating RGC axons were labeled with
130 anterogradely transported cholera toxin subunit B (CTB) conjugated with Alexa Fluor 594, which was
131 injected into the vitreous humor 2 days prior to tissue harvest (Fig. 1A). The fixed optic nerves were first
132 tissue cleared to be transparent as previously described (*12*) and then axons were imaged with confocal
133 microscopy. The results showed that very limited optic nerve regeneration occurred in wild type mice
134 infected with AAV2-Cre. In contrast, there was greatly enhanced optic nerve regeneration in myosin IIA/B
135 dKO mice (Fig. 1A, B). In the majority of optic nerves, regenerating axons reached 750 μm from the crush
136 site. To further determine if myosin IIA/B dKO led to sustained promoting effect on optic nerve
137 regeneration, we assessed optic nerve regeneration 4 weeks after the ONC. We found that at 4 weeks post
138 ONC myosin IIA/B dKO significantly increased not only the lengths but also the number of regenerating
139 axons, indicating continued axon regeneration along time. Specifically, most optic nerves had regenerating
140 axons reaching 2000 μm from the crush site (Fig. 1B). In addition to counting axon numbers at different
141 distances from the crush site, we also quantified the lengths of the top 5 longest regenerating axons in
142 each condition. The result showed that in control condition the lengths of the top 5 axons remained
143 unchanged at 2 and 4 weeks, whereas the top 5 axons of myosin IIA/B dKO RGCs continued to grow
144 from 2 to 4 weeks (Fig. 1C). Both quantification results demonstrated that knocking out myosin IIA/B in
145 RGCs led to sustained optic nerve regeneration at the same speed up to 4 weeks. When RGC survival rates
146 were assessed, myosin IIA/B dKO showed no effect (Fig. 1D, E), indicating that it promoted optic nerve
147 regeneration by enhancing axon extension rather than protecting RGCs from ONC-induced cell death.

148 Collectively, these results demonstrated clearly that knocking out myosin IIA/B was sufficient to induce
149 robust and sustained optic nerve regeneration without affecting cell survival.
150
151 **Knocking out non-muscle myosin IIA/B acted synergistically with Lin28a overexpression to**
152 **promote long-distance optic nerve regeneration**
153 Our recent study showed that overexpression of Lin28 in RGCs induced robust and sustained optic
154 nerve regeneration via regulation of gene expression and enhanced intrinsic axon regeneration ability (*12*).
155 Therefore, we tested if combining myosin IIA/B dKO, which alters axonal cytoskeletal dynamics, with
156 Lin28 overexpression, which controls gene expression, could have combinatory promoting effect on optic
157 nerve regeneration. The results showed that either myosin IIA/B dKO or Lin28a overexpression alone
158 could lead to robust optic nerve regeneration 2 weeks after ONC (Fig. 2A, B). When both treatments were
159 combined, optic nerve regeneration was greatly enhanced, with the longest length reaching 3.5mm from
160 the crush site (Fig. 2A, B). In particular, either myosin IIA/B dKO or Lin28a overexpression RGCs had
161 almost no regenerating axons growing beyond 1.75 mm from the crush site. In contrast, in the combinatory
162 treatment group there were significant number of regenerating axons at 3 mm and the longest axons
163 reached up to 3.5 mm (Fig. 2A, B). Because the dehydration process in the tissue clearing approach results
164 in 18% of shrinkage in nerve lengths (*12*), the real lengths of the longest regenerating axons were more
165 than 4 mm. Indeed, in about half of nerves in the combinatory group the longest regenerating axons almost
166 reached the optic chiasm (Fig. 2A and Fig. S4) 2 weeks after ONC. This result suggested that myosin
167 IIA/B dKO and Lin28a acted synergistically to promote long-distance optic nerve regeneration. Similarly,
168 we quantified the average distances of the top 5 longest regenerating axons in each condition. The results
169 showed that the longest regenerating axons in the combinatory group were markedly longer than either

170 the myosin IIA/B dKO or Lin28a overexpression group (Fig. 2C). To better show the regenerating axons
171 in the tissue cleared transparent optic nerves, we created a 3D animation of an optic nerve (Movie S1).
172

173 **Knocking out non-muscle myosin IIA/B in RGCs did not significantly affect known optic nerve**
174 **regeneration signaling pathways**

175 In our previous study (*21*), we showed that treating adult sensory neurons cultured on CSPGs with
176 the myosin II inhibitor, blebbistatin, could induce halted axon to regrow within minutes. Conversely,
177 washing out blebbistatin stopped axon growth in a very short time. Such rapid response to blebbistatin in
178 both ways indicated that inhibition of myosin II promoted axon growth through its direct effects on the
179 growth cone cytoskeleton without affecting signaling events in the neuronal soma. To test this idea, we
180 examined how myosin IIA/B dKO affected two well-known pathways governing the intrinsic axon
181 regeneration ability, the activation of mTOR, marked by increased level of phospho-S6 (pS6), and the
182 inactivation of GSK3β, marked by phosphorylation of its serine 9 residue (pGSK3β), at 2 weeks after
183 ONC. Previous studies have shown that most identified molecules promoting optic nerve regeneration act
184 via either of these pathways, including Pten knockout (*9*), Akt overexpression (*22, 23*), Lin28
185 overexpression (*12*), osteopontin overexpression (*24*), SOCS3 deletion (*10*), melanopsin overexpression
186 (*25*), HDAC5 manipulation (*26*), and direct modulation of mTOR (*27*) or GSK3β signaling (*22*). For
187 mTOR activation, we examined the level of pS6 in RGCs under different conditions. The results showed
188 that knocking out myosin IIA/B had no effect on pS6 level, whereas Lin28a overexpression markedly
189 increased the level of pS6 in RGCs (Fig. 3A). Quantification demonstrated that the percentage of pS6
190 positive ($pS6^+$) RGCs increased by nearly 8 folds in the Lin28a overexpression group compared to that in
191 the wild type group, whereas myosin IIA/B dKO had no effect (Fig. 3B). To provide a more objective
192 measurement of pS6 level in RGCs, we also quantified the average fluorescence intensity of pS6 staining

193 in all Tuj1 positive RGCs. The results showed that myosin IIA/B dKO actually slightly reduced the pS6
194 level compared to that of the wild type group. In contrast, Lin28a overexpression greatly increased the
195 pS6 level (Fig. 3C). Lastly, we quantified the average fluorescence intensity of pS6 staining only in $pS6^+$
196 RGCs under different conditions. Similarly, there was no significant difference between wild type and
197 myosin IIA/B dKO RGCs, whereas the Lin28a overexpression group had a much higher value (Fig. 3D).
198 For GSK3β inactivation, we found that there were very few wild type RGCs showing positive
199 staining of pGSK3β, and knocking out myosin IIA/B had no impact on it (Fig. 3E, F). In contrast, Lin28a
200 overexpression increased the percentage of pGSK3β positive ($pGSK3\beta^+$) RGCs by about 6 folds (Fig. 3F).
201 The average fluorescence intensity of pGSK3β staining in all Tuj1 positive RGCs was not affected by
202 myosin IIA/B dKO, whereas Lin28a overexpression greatly increased the pGSK3β level (Fig. 3G). When
203 the average fluorescence intensity of pGSK3β was quantified only in $pGSK3\beta^+$ RGCs, the level of
204 pGSK3β was significantly decreased in myosin IIA/B dKO group compared with that in the wild type
205 group. The level of pGSK3β in the Lin28a overexpression group was still the highest (Fig. 3H).
206 Taken together, these results provided clear and strong evidence that knocking out myosin IIA/B
207 had no effects on two well-known signaling pathways occurred in the neuronal soma supporting intrinsic
208 regenerative ability of optic nerves.
209
210 **Knocking out non-muscle myosin IIA/B in sensory neurons did not significantly affect known**
211 **regeneration associated genes and pathways**
212 Double knockdown of myosin IIA/B in sensory neurons drastically promoted regenerative axon
213 growth over CSPGs or CNS myelin (*21*), similar to our finding in RGC axons. Therefore, we generated
214 *Advillin-Cre: myosin IIA/B$^{f/f}$* mice, in which myosin IIA/B were conditionally knocked out in sensory
215 neurons, to explore if myosin IIA/B dKO in neurons affected known regeneration associated genes and

216 pathways. We performed sham surgery or bilateral sciatic nerve injury (SNI) on these mice or wild type
217 mice. Three days later, we collected lumbar 4 and 5 dorsal root ganglia (L4/5 DRGs) and isolated mRNA
218 and protein for RNA-seq and western blot analyses. As expected, mRNA levels of myosin IIA/B in L4/5
219 DRGs of *Advillin-Cre: myosin IIA/B*$^{f/f}$ mice were lowered (Fig. 4A). Pearson correlation coefficient of
220 gene expression indicated by FPKM (Fragments Per Kilobase of exon model per Million mapped reads)
221 among different samples showed that under the same treatment (sham or SNI), the two wild type replicates
222 were quite similar to the two dKO replicates (Fig. 4B). When the numbers of differentially expressed
223 genes (DEGs) were compared, we found SNI significantly altered the mRNA levels of nearly 2000 genes,
224 whereas myosin IIA/B dKO caused little change. Specifically, the number of DEGs between wild type
225 neurons and myosin IIA/B dKO neurons was actually equivalent to that between the two replicates within
226 each condition (Fig. 4C). These results indicated that myosin IIA/B dKO *per se* did not significantly
227 change the transcriptome in sensory neurons. In addition, in wild type and myosin IIA/B dKO neurons,
228 we closely examined and compared the FPKMs of many classic regeneration-associated genes (RAGs)
229 and genes well-known to control axon regeneration, such as *Atf3*, *Sox11*, *Lin28a*, *Gap43*, *Pten*, *Klf9*, and
230 *Rab27*, etc (*12, 28-32*). The results showed that the mRNA levels of these genes were up- or
231 downregulated by SNI as expected, but were not largely affected by myosin IIA/B dKO (Fig. 4D, E).
232 Gene ontology analysis of DEGs between different conditions revealed that SNI stimulated many neuron-
233 related programs (Fig. 4G), whereas myosin IIA/B dKO induced gene expression change had no specific
234 connection with neurons or axon regeneration (Fig. 4H). Lastly, we directly examined the protein levels
235 of several genes and pathways regulating axon regeneration by western blot and found that in either
236 uninjured or injured condition, myosin IIA/B dKO did not change the protein levels of Atf3, c-Jun, Gap43
237 or c-Myc (Fig. 4F). Moreover, consistent with our RGC immunostaining results, myosin IIA/B dKO had
238 no impact on mTOR or GSK3β pathway (Fig. 4F) in sensory neurons. Taken together, these results further

239 supported that myosin IIA/B dKO induced optic nerve regeneration was unlikely to be caused by enhanced
240 intrinsic axon regeneration ability.
241
242 **Knocking out non-muscle myosin IIA/B in RGCs changed axon tip morphology and regenerating**
243 **axon trajectory**
244 To better understand the cellular mechanisms by which myosin IIA/B knockout promoted optic
245 nerve regeneration locally at the axons, we first performed detailed analysis of axonal tip morphologies
246 in wild type and myosin IIA/B dKO optic nerves 2 and 4 weeks after ONC. Based on a previous study
247 (*33*), there are mainly three types of dynamic axonal tip morphologies in vivo. One is the retraction bulb
248 (Fig. 5A, C), which is the hallmark structure of dystrophic axons that failed to regenerate (*18, 20*). The
249 other two are growth-competent growth cones with two different end shapes (Fig. 5A, C). We found that
250 in wild type optic nerves, a significant percentage of axons had retraction bulbs at their ends, whereas
251 knocking out myosin IIA/B in RGCs almost abolished the formation of retraction bulbs (Fig. 5A, B). Most
252 regenerating axons in the myosin IIA/B knockout nerves had growth-competent growth cones, indicating
253 that deleting myosin IIA/B efficiently transformed dystrophic axon tips into growth cones and rendered
254 subsequent axon regeneration.
255 The tissue clearing and confocal imaging of whole-mount optic nerves allowed us to visualize the
256 bona fide morphology of regenerating axons. Thus, we next examined how myosin IIA/B knockout
257 influenced the axon extension trajectories 4 weeks after ONC. In wild type nerves, the majority of axons
258 followed a wandering path with many curves and backward turns (U-turns), which resulted in very
259 inefficient axon regeneration towards the distal optic nerve. In contrast, in myosin IIA/B dKO nerves,
260 most regenerating axons were straight with significantly reduced U-turns (Fig. 5D-F and Fig. S5, S6),
261 indicating a higher efficiency of axon regeneration towards the distal end. Together, we think that

262 enhanced optic nerve regeneration induced by myosin IIA/B dKO was achieved through 1) switching
263 retraction bulbs into growth-competent growth cones, and 2) more efficient axon regeneration with
264 straighter axon growth and less U-turns.
265

266 **Knocking out non-muscle myosin IIA/B in RGCs after optic nerve crush could also induce optic**
267 **nerve regeneration**

268 To investigate the translational potentials of myosin IIA/B knockout, we tested if post-injury
269 deletion of myosin IIA/B in RGCs could also promote axon regeneration. We first performed the ONC on
270 wild type and *myosin IIA/B*$^{f/f}$ mice, and one day after that, we injected AAV2-Cre into the vitreous humors
271 of these mice. The optic nerve regeneration was assessed 3 weeks after the ONC (Fig. 6A). The result
272 showed that only a small number of axons regenerated for a limited distance in the wild type optic nerves.
273 In contrast, a large number of regenerating axons were observed in dKO optic nerves (Fig. 6B). Most dKO
274 optic nerves had regenerating axons reaching 1500 μm from the crush site, although the most noticeable
275 difference between the two groups was found at 500-1250 μm from the crush site (Fig. 6B). Such a result
276 demonstrated clearly that post-injury treatment with myosin IIA/B knockout could successfully induce
277 axon regeneration in injured optic nerves, indicating myosin IIA/B knockout may potentially be applied
278 to translational practices in treating diseases and injuries involving axon damage.

Discussion

In addition to diminished intrinsic axon regeneration capacity regulated by changes in gene expression during neuronal maturation, dystrophic growth cone with disruptive cytoskeletal dynamics is another key intrinsic barrier for successful CNS axon regeneration (*18*). Although it has been well recognized that modulation of axonal cytoskeleton would be a plausible approach to enhance CNS axon regeneration, very few studies have shown direct and convincing results. Two previous elegant studies (*34, 35*) have shown that moderate stabilization of microtubules with taxol or epothilone B could promote axon regeneration after the spinal cord injury. The promoting effects were achieved through decreased glial scar formation, which rendered the lesion site more permissive, and improved microtubule protrusion in the growth cones of the injured axons. However, the promoting effects were moderate with regenerating axons only entering the injury site. Similarly, after optic nerve injury low dose taxol treatment alone had little promoting effect on axon regeneration (*36*).

In this study we provided clear evidence that knocking out myosin IIA/B in RGCs alone was sufficient to induce robust and sustained optic nerve regeneration. Our previous in vitro study (*21*) demonstrated that deleting myosin IIA/B acted locally at the growth cone without affecting signaling events at the neuronal soma and gene transcription. Specifically, we showed that inhibiting myosin II activity resulted in reduced level of actin filaments in the growth cone. Retrograde flow of F-actin driven by myosin II acts as a dynamic barrier for microtubule protrusion in the growth cone. As a result, inhibition of myosin II led to significant microtubule protrusion towards the leading edge of the growth cone and increased axon growth rate. Moreover, the promoting effects of myosin II inhibition over inhibitory substrates (CSPGs) occurred within minutes and was reversible, further supporting the effects were local. Indeed, here we carefully examined how RGC axonal morphology and trajectory were affected after myosin IIA/B knockout. The inability of mature CNS axon to form a growth-competent growth cone in

302 the inhibitory environment after injuries is a hallmark of regeneration failure (*18, 20*). In most cases, after
303 CNS injuries, a bulb-like structure is formed at the tip of the injured axon, called the retraction bulb (*33*).
304 In wild type mice, very limited optic nerve regeneration was observed, and retraction bulbs were more
305 often observed at the tips of the axons. In contrast, in myosin IIA/B dKO nerves, very few retraction bulbs
306 were identified, while growth-competent growth cones could be found at almost all axonal tips. The results
307 indicated that deleting myosin IIA/B was an efficient strategy to transform retraction bulbs into growth
308 cones, likely achieved through slowed retrograde flow of actin filaments and the subsequent protrusion of
309 microtubules in the dystrophic growth cones. In addition, confocal microscopy of tissue cleared whole-
310 mount optic nerves allowed us to trace the trajectories of regenerating axons. We found that in the wild
311 type group, the majority of axons showed wandering trajectories with many kinks and U-turns, likely due
312 to the inhibitory substrates in the optic nerve. As a result, such axon extension resulted in very inefficient
313 axon regeneration. When myosin IIA/B were knocked out, most axons followed a straighter path with
314 reduced U-turns, indicating myosin IIA/B deletion could overcome inhibitory cues and greatly enhance
315 regeneration efficiency.

316 We also examined two well-known signaling pathways in RGCs, mTOR activation and GSK3β
317 inactivation, which occur in the neuronal soma to support the intrinsic axon regeneration ability. The
318 results showed that deleting myosin IIA/B had no effects on these two pathways, suggesting that the
319 intrinsic axon regeneration ability of RGCs might not be elevated. In contrast, overexpression of Lin28a,
320 which promotes optic nerve regeneration by enhancing the intrinsic axon regeneration ability, led to
321 marked activation of mTOR and inactivation of GSK3β in RGCs. Next, by using sensory neuron specific
322 myosin IIA/B conditional knockout mice, we explored how deleting myosin IIA/B affected sensory
323 neuron transcriptome. The results showed that deleting myosin IIA/B did not significantly change the
324 transcription profile in sensory neurons. More importantly, when the transcription levels of many known

325 RAGs were examined, we found that peripheral axotomy significantly changed their mRNA levels,
326 whereas knocking out myosin IIA/B had little effects. Lastly, we directly examined the protein levels of
327 selected RAGs and signaling mediators with western blot. Similarly, knocking out myosin IIA/B had little
328 effects, whereas peripheral axotomy showed significant impact. Together, these results suggested that
329 myosin IIA/B knockout promoted optic nerve regeneration without affecting gene transcription and the
330 intrinsic axon regeneration ability. Collectively, our study suggested that deleting myosin IIA/B promoted
331 optic nerve regeneration by efficiently transforming retraction bulbs into active growth cones and more
332 efficient axon extension within the inhibitory CNS environment.

333 Long-distance axon regeneration is one of the most important aspects and a prerequisite for
334 successful functional recovery after neural injuries. Several previous studies (*37-39*), including ours (*12*),
335 have shown that combined manipulation of multiple genes/pathways usually had additive or synergistic
336 promoting effects on optic nerve regeneration. Given sufficient time, some axons could even regrow back
337 to their targets in the brain and led to partial function recovery (*39*). Here we showed that combining
338 myosin IIA/B knockout with Lin28a overexpression resulted in surprisingly long-distance optic nerve
339 regeneration. Two weeks after ONC, regenerating axon reached up to 3.25 mm from the crush site (nearly
340 4 mm in real distance considering 18% shrinkage due to the tissue clearing process (*12*)) without
341 enhancing the RGC survival rate. The longest regenerating axons were about 4.3 mm and close to the
342 optic chiasm. To our knowledge, such a distance was comparable with those in most previously published
343 studies using combinatory approaches. For instance, combined knockout of Pten and SOCS3, together
344 with CNTF, led to optic nerve regeneration up to 3 mm from the crush site 2 weeks after ONC (*37*).
345 Moreover, combination of Zymosan, c-AMP, and Pten deletion could promote optic nerve regeneration
346 to 3 mm from the crush site in 2 weeks (*38*). The effectiveness of the combinatory approach will be optimal
347 if each gene/pathway acts independently. Our previous study found that Lin28 overexpression could

348 induce optic nerve regeneration by enhancing the intrinsic growth ability of RGCs (*12*). A recent study
349 confirmed that specific expression of Lin28 in RGCs could lead to significant optic nerve regeneration. In
350 addition, it also revealed that apart from its direct effect on RGCs, Lin28 specifically expressed in
351 amacrine cells could enhance IGF1-induced optic nerve regeneration by suppressing hyperactivity of
352 amacrine cells induced by optic nerve injury (*13*). As such, Lin28a and myosin II could act in distinct
353 neuronal compartments with diverse cellular mechanisms, resulting in a powerful combination. Because
354 AAV2 also infected amacrine cells, we could not completely rule out the possibility that knocking out
355 myosin IIA/B in amacrine cells somehow contributed to the observed results. Although the number of
356 long-distance regenerating axons observed in this study was relatively low, it was likely due to the poor
357 survival of RGCs, and the different regeneration capacities among RGC subpopulations (*24*). Thus,
358 myosin II knockout can be a new effective option for combination strategies, and future studies combining
359 myosin II knockout with other regeneration approaches, as well as enhanced RGC survival, may
360 potentially lead to large number of axons regenerating back to their original targets in the brain and gain
361 recovery of lost visual function.

362 Here we also showed that deleting myosin IIA/B in RGCs after the optic nerve injury could induce
363 robust optic nerve regeneration, indicating that myosin IIA/B deletion or inhibition has the potential to be
364 practically used in the treatment of nerve injury. Moreover, the availability of water soluble and stable
365 pharmacological inhibitor of myosin II (*40*) would make future translational applications possible to repair
366 axonal injuries induced by glaucoma, spinal cord injury, traumatic brain injury, and neurodegenerative
367 diseases.

368 **Materials and Methods**

369 **Mice**

370 All animal experiments were conducted in accordance with the protocol approved by the
371 Institutional Animal Care and Use Committee of the Johns Hopkins University. The *Myh9*$^{f/f}$
372 (stock#032096-UNC) and *Myh10*$^{f/f}$ (stock#016981-UNC) mouse strains were obtained from Mutant
373 Mouse Resource and Research Center (MMRRC) at University of North Carolina at Chapel Hill, an NIH-
374 funded strain repository, and were donated to the MMRRC by Robert S. Adelstein, M.D., National Heart,
375 Lung, and Blood Institute (NHLBI). The two lines were crossed to generate *Myh9*$^{f/f}$*: Myh10*$^{f/f}$ mice.
376 *Advillin-Cre* mouse line was a kind gift from Dr. Fan Wang's laboratory at Duke University, and was
377 crossed with *Myh9*$^{f/f}$*: Myh10*$^{f/f}$ to get *Advillin-Cre: Myh9*$^{f/f}$*: Myh10*$^{f/f}$ conditional knockout mice. The
378 tdTomato reporter line (stock#007909) was purchased from The Jackson Laboratory. Adult mice (6 weeks)
379 of both sexes were used. Genotypes of the mice were determined by PCR using primers provided by
380 MMRRC and The Jackson Laboratory. All animal surgeries were performed under anesthesia induced by
381 intraperitoneal injection of ketamine (100 mg/kg) and xylazine (10 mg/kg) diluted in sterile saline. Details
382 of the surgeries are described below.

383

384 **Construct**

385 The pAAV-Ef1a-Lin28a-FLAG plasmid was constructed in a previous study (*12*). Briefly, the
386 Lin28a-FLAG open reading frame with a 5' BamHI and a 3' EcoRV restriction sites was synthesized
387 (codon optimized, gBlocks of Integrated DNA Technologies) and used for replacing the EYFP open
388 reading frame in pAAV-Ef1a-EYFP, to obtain the pAAV-Ef1a-Lin28a-FLAG plasmid. pAAV-Ef1a-
389 EYFP was a kind gift from Dr. Hongjun Song's laboratory at University of Pennsylvania. All restriction

390 enzymes and T4 DNA ligase were purchased from New England Biolabs. Plasmids were amplified using
391 DH5α competent cells (Thermo Fisher Scientific) and purified with Endofree plasmid maxi kit (Qiagen).
392

393 **Optic nerve regeneration model**

394 Intravitreal viral injection, optic nerve crush and RGC axon labeling were performed as previously
395 described (*9*). Briefly, under anesthesia, 1.5 µl of AAV2 virus was injected into the right vitreous humor
396 of a mouse with a Hamilton syringe (32-gauge needle). The position and direction of the injection were
397 well-controlled to avoid injury to the lens. Two weeks later, the right optic nerve of the mouse was exposed
398 intraorbitally and crushed with Dumont #5 fine forceps (Fine Science Tools) for 5 s at approximately 1
399 mm behind the optic disc. To label RGC axons in the optic nerve, 1.5 µl of Alexa Fluor 594-conjugated
400 CTB (2 µg/µl, Thermo Fisher Scientific) was injected into the right vitreous humor with a Hamilton
401 syringe (32-gauge needle) 2 days before the mouse was sacrificed by transcardial perfusion under
402 anesthesia. The right optic nerve and bilateral retinas were dissected out and post-fixed in 4% PFA
403 overnight at 4°C. AAV2-Cre (SL100813) was purchased from SignaGen Laboratories. AAV2-Lin28a-
404 FLAG was also packaged by SignaGen Laboratories. All viruses used had titers over 1 x 10^{13} gc/ml.

405 For post-injury treatment model, all procedures were done in the same way except the intravitreal
406 viral injection was conducted one day after the optic nerve crush.

407 **Optic nerve dehydration and clearing**

408 Dehydration and clearing of optic nerves were done based on previous studies (*14, 41*). Briefly,
409 fixed optic nerves were first dehydrated in increasing concentrations of tetrahydrofuran (50%, 70%, 80%,
410 100% and 100%, v/v % in distilled water, 20 min each, Sigma-Aldrich) and then cleared in a solution of
411 benzyl alcohol and benzyl benzoate (BABB, 1:2, Sigma-Aldrich). Incubations were done on an orbital
412 shaker at room temperature. The nerves were stored in BABB in the dark at room temperature.

413

414 **Analysis of RGC axon regeneration**

415 Tissue cleared whole-mount optic nerves were imaged with a 20x objective on a Zeiss 800
416 confocal microscope. For each optic nerve, Z-stack and tiling (10% overlap) functions were used to
417 acquire stacked 2-µm-thick planes of the whole area of interest and the tiles were stitched.

418 To quantify the number of regenerating axons in each optic nerve, every 8 consecutive planes were
419 Z-projected (maximum intensity) to generate a series of Z-projection images of 16-µm-thick optical
420 sections. At each 250-µm interval from the crush site, the number of CTB-labeled axons was counted in
421 each Z-projection image and summed over all optical sections.

422 To quantify the average length of top 5 longest axons of each optic nerve, all stitched 2-µm-thick
423 planes were Z-projected (maximum intensity) to obtain a single Z-projection image of the nerve. Top 5
424 longest regenerating axons were manually traced from the axonal tips to the crush site using the Fiji
425 software (NIH) to acquire the lengths of the axons.

426

427 **Immunohistochemistry of whole-mount retinas**

428 Fixed retinas were first radially cut into a petal shape (4 incisions) and blocked with PBST (1%)
429 containing 10% goat serum for 1 hr at room temperature. The retinas were then sequentially stained with
430 primary antibodies overnight at 4°C, and corresponding Alexa Fluor-conjugated secondary antibodies
431 (1:500, Thermo Fisher Scientific) for 2 hr at room temperature. All antibodies were diluted with the
432 blocking buffer. Following each antibody incubation, the retinas were washed with PBST (0.3%) for 4
433 times (15 min each). After the last wash, the retinas were mounted onto slides with Fluoroshield (Sigma-
434 Aldrich). Fluorescent images of the flat-mounted retinas were acquired with a 20x objective on a Zeiss
435 800 confocal microscope.

436

437 **Analysis of RGC transduction rate**

438 To quantify RGC transduction rate, uninjured right retinas (no optic nerve crush) were taken from
439 transcardially perfused *Myh9*$^{f/f}$*: Myh10*$^{f/f}$ mice 2 weeks after intravitreal AAV2-Cre injection. The retinas
440 were stained with mouse anti-tubulin β3 (Tuj1, 1:500, BioLegend) and rabbit anti-Cre recombinase (1:100,
441 Cell Signaling Technology) antibodies following the steps mentioned above (see Immnunohistochemistry
442 of whole-mount retinas). Five to eight fields under 20x objective were randomly obtained from the
443 peripheral regions of each flat-mounted retina. For each mouse, RGC transduction rate was calculated by
444 dividing the total number of Cre^{+}/Tuj1^{+} cells in all fields by the total number of Tuj1^{+} cells in all fields.
445 Only cells in the ganglion cell layer were counted.

446

447 **Analysis of RGC survival rate**

448 To quantify RGC survival rate, C57Bl6/J and *Myh9*$^{f/f}$*: Myh10*$^{f/f}$ mice injected with AAV2-Cre were
449 transcardially perfused 2 weeks after optic nerve crush and both retinas of each mouse were collected. The
450 retinas were stained with mouse anti-tubulin β3 antibody (Tuj1, 1:500, BioLegend) following the steps
451 mentioned above (see Immnunohistochemistry of whole-mount retinas). Seven or eight fields under 20x
452 objective were randomly taken from the peripheral regions of each flat-mounted retina. For each mouse,
453 RGC survival rate was calculated by dividing the average number of Tuj1^{+} cells in one field in the injured
454 retina (right) by that in the uninjured retina (left). Only cells in the ganglion cell layer were counted.

455

456 **Immunohistochemistry of retinal sections**

457 Fixed retinas were sectioned with a cryostat (10 μm) and the retinal sections were warmed on a
458 slide warmer at 37°C for 1 hr. Sections were rinsed once in PBS, soaked in 100°C citrate buffer (pH 6)

459 for 15 min, let to cool in the buffer to room temperature and then washed twice (5 min each) in PBS. After
460 being blocked with PBST (0.3%) containing 10% goat serum at room temperature for 1 hr, the sections
461 were stained with primary antibodies against target molecules overnight at 4 °C, followed by
462 corresponding Alexa Fluor-conjugated secondary antibodies (1:500, Thermo Fisher Scientific) at room
463 temperature for 1 hr. All antibodies were diluted with the blocking buffer. The sections were washed for
464 4 times (5, 5, 10, 10 min) with PBST (0.3%) following each antibody incubation and finally mounted with
465 DAPI Fluoromount-G (SouthernBiotech). Fluorescent images of the retinal sections were taken with a
466 CCD camera connected to a Zeiss inverted fluorescence microscope controlled by AxioVision software.
467

468 **Analysis of myosin IIB level in RGCs**

469 To analyze myosin IIB level in RGCs, both retinas (uninjured) of each mouse were taken from
470 transcardially perfused *Myh9*$^{f/f}$*: Myh10*$^{f/f}$ mice 2 weeks after intravitreal AAV2-Cre injection and sectioned.
471 The retinal sections were stained with mouse anti-tubulin β3 (Tuj1, 1:500, BioLegend) and rabbit anti-
472 myosin IIB (1:100, Thermo Fisher Scientific) antibodies following the steps mentioned above (see
473 Immnunohistochemistry of retinal sections).

474 To quantify the fluorescence intensity of myosin IIB in all RGCs, at least 7 non-adjacent retinal
475 sections acquired with identical imaging configurations were analyzed for each retina. Fluorescence
476 intensity was measured using the "outline spline" function of AxioVision and the background fluorescence
477 intensity was subtracted.
478

479 **Analysis of S6 and GSK3β phosphorylation**

480 To analyze S6 and GSK3β phosphorylation in RGCs, C57Bl6/J and *Myh9*$^{f/f}$*: Myh10*$^{f/f}$ mice injected
481 with AAV2-Cre, and *Myh9*$^{f/f}$*: Myh10*$^{f/f}$ mice injected with AAV2-Lin28a-FLAG were transcardially

482 perfused 2 weeks after optic nerve crush and the right retina of each mouse was collected and sectioned.
483 The retinal sections were stained with mouse anti-tubulin β3 antibody (Tuj1, 1:500, BioLegend), and
484 rabbit anti-pS6 Ser235/236 (1:200, Cell Signaling Technology) or rabbit anti-pGSK3β Ser9 (1:200, Cell
485 Signaling Technology) antibody following the steps mentioned above (see Immnunohistochemistry of
486 retinal sections).

487 To quantify the percentage of $pS6^+$ or $pGSK3\beta^+$ RGCs, at least 363 or 434 RGCs from at least 7
488 non-adjacent retinal sections from each mouse were analyzed. For each mouse, the percentage of $pS6^+$ or
489 $pGSK3\beta^+$ RGCs was calculated by dividing the number of $pS6^+/Tuj1^+$ or $pGSK3\beta^+/Tuj1^+$ cells by the
490 number of $Tuj1^+$ cells. Only cells in the ganglion cell layer were counted.

491 The relative fluorescence intensity of each RGC was calculated by dividing the fluorescence
492 intensity of the RGC by that of its adjacent tissue. To quantify the fluorescence intensity of pS6 or pGSK3β
493 in all RGCs, 20 retinal sections acquired with identical imaging configurations from at least 2 mice were
494 analyzed for each group. To quantify the fluorescence intensity of pS6 or pGSK3β in S6-activated or
495 GSK3β-inactivated RGCs, at least 40 RGCs with identical imaging configurations from at least 2 mice
496 were analyzed for each group. Fluorescence intensity of RGCs were measured using the "outline spline"
497 function of AxioVision.

498

499 **Sciatic nerve injury model**

500 Under anesthesia, bilateral sciatic nerves of a mouse were exposed and transected with spring
501 scissors right below pelvis. Nerves were only exposed but not transected for a sham surgery. Three days
502 after the surgery, the mouse was euthanized and bilateral L4/5 DRGs were collected and used for total
503 RNA or protein extraction.

504

505 **mRNA sequencing and data analysis**

506 Total RNA was isolated with RNeasy mini kit (Qiagen) and RNA integrity was determined by
507 Agilent 2100 bioanalyzer and RNA 6000 Nano kit (Agilent Technologies). Paired-end libraries were
508 synthesized using the TruSeq RNA library preparation kit (Illumina). Briefly, mRNA molecules were
509 purified using oligo dT-attached magnetic beads. Following purification, the mRNA molecules were
510 fragmented into small pieces using divalent cations at 94°C for 8 min. The cleaved RNA fragments were
511 reversely transcribed into first strand cDNA using reverse transcriptase and random primers. This was
512 followed by second strand cDNA synthesis using DNA Polymerase I and RNase H. These cDNA
513 fragments then went through an end repair process, the addition of a single base, and the ligation of the
514 adapters. The products were then purified and enriched with PCR to obtain the final cDNA library.
515 Purified libraries were quantified by Qubit 2.0 fluorometer (Thermo Fisher Scientific) and validated by
516 Agilent 2100 bioanalyzer (Agilent Technologies) to confirm the insert size and calculate the mole
517 concentration. Cluster was generated by cBot with the library diluted to 10 pM and sequencing was done
518 on HiSeq 2500 (Illumina).

519 Sequencing raw reads were preprocessed by filtering out rRNA reads, sequencing adapters, short-
520 fragment reads and other low-quality reads using Seqtk (github.com/lh3/seqtk). Hisat2 (version 2.0.4) (*42*)
521 was used to map the cleaned reads to the mouse GRCm38.p4 (mm10) reference genome with two
522 mismatches. After genome mapping, Stringtie (version 1.3.0) (*43, 44*) was run with a reference annotation
523 to generate FPKM (Fragments Per Kilobase of exon model per Million mapped reads) values for known
524 gene models (*45*). Differentially expressed genes were identified using edgeR (*46*). The *P* value
525 significance threshold in multiple tests was set by the false discovery rate (FDR) (*47, 48*). The cut-off for
526 differentially expressed genes was set as $P < 0.05$ and |log2fold change| > 1. For genes used for gene
527 ontology (GO) analyses, an additional cut-off of average FPKM > 1 in at least one condition was applied.

528 GO analysis was done using DAVID Bioinformatics Resources 6.8 (*49, 50*). GO terms came from
529 biological process, cellular component and molecular function categories.
530
531 **Western blot analysis**
532 Total protein was extracted from L4/5 DRGs or retinas using the RIPA buffer containing protease
533 inhibitor cocktail (Sigma-Aldrich) and phosphatase inhibitor cocktail (Sigma-Aldrich). Identical amount
534 of total protein from each condition was then separated by 4-12% gradient SDS-PAGE gel electrophoresis
535 and transferred onto polyvinylidene fluoride membranes. After being blocked with TBST (1%) containing
536 5% blotting-grade blocker (Bio-Rad), the membranes were incubated overnight with primary antibodies
537 against target molecules at 4 °C, followed by corresponding HRP-linked secondary antibodies (1:2000,
538 Cell Signaling Technology) for 1 hr at room temperature. All antibodies were diluted with blocking buffer.
539 The membranes were washed with TBST (1%) for four times (5, 5, 10, 10 min) after each antibody
540 incubation. Rabbit primary antibodies against myosin IIA (1:1000), Atf3 (1:1000), Gap43 (1:1000), c-Jun
541 (1:1000), c-Myc (1:1000), pAkt Ser473 (1:2000), pGSK3β Ser9 (1:1000), pS6 Ser235/236 (1:2000) were
542 purchased from Cell Signaling Technology. Mouse anti-β-actin primary antibody (1:5000) was from
543 Sigma-Aldrich.
544
545 **Analysis of axonal tip morphology**
546 The method was derived from a previous study (*33*). For each optic nerve, top 10 longest axons
547 were first identified in the Z-projection image of the nerve. Then the maximum diameter of each axonal
548 tip and the diameter of the cylindrical shaft of the corresponding axon were measured using Fiji software
549 (NIH), and a tip/shaft ratio was calculated. An axonal tip was defined as a retraction bulb if its tip/shaft
550 ratio was over 4. Otherwise, it was defined as a growth cone.

551

552 **Analysis of axon extension efficiency**

553 For each optic nerve, a 250-μm-long region with equivalent number of axons in the Z-projection
554 image of the nerve was used for analysis. All traceable axons within this region were manually traced. For
555 each axon, the length (covered distance on its trajectory) and the displacement (distance along the
556 longitudinal axis of the nerve, sometimes could be zero or negative) between the start point and the end
557 point were measured using Fiji software (NIH). The extension efficiency of each nerve was calculated by
558 dividing the summed displacement by the summed length of all axons.

559

560 **Analysis of U-turn rate**

561 For each optic nerve, top 15 longest axons were identified in the Z-projection image of the nerve
562 and their trajectories near the axonal tips were traced. A U-turn was defined when the angle between the
563 final direction of the axonal tip and the positive longitudinal axis of the optic nerve was larger than 90
564 degrees. U-turn rate of each nerve was calculated by dividing the number of axons that made U-turns by
565 15.

566

567 **Quantification and statistical analysis**

568 Statistical analyses were done with GraphPad Prism 7 and the significance level was set as $P <$
569 0.05. Data are represented as mean ± SEM unless specifically stated. For comparisons between two groups,
570 two-tailed unpaired or paired t test was used. For comparisons among three or more groups, one-way
571 ANOVA followed by Tukey's multiple comparisons test was used to determine the statistical significance.
572 Fisher's exact test was used to test contingency tables. All details regarding statistical analyses, including
573 the tests used, *P* values, exact values of n, definitions of n, are described in figure legends.

574 **Reference and Notes**

575 1. Z. He, Y. Jin, Intrinsic Control of Axon Regeneration. *Neuron* **90**, 437-451 (2016).

576 2. M. Curcio, F. Bradke, Axon Regeneration in the Central Nervous System: Facing the Challenges
577 from the Inside. *Annu Rev Cell Dev Biol* **34**, 495-521 (2018).

578 3. S. David, A. J. Aguayo, Axonal elongation into peripheral nervous system "bridges" after central
579 nervous system injury in adult rats. *Science* **214**, 931-933 (1981).

580 4. J. W. Fawcett, The Paper that Restarted Modern Central Nervous System Axon Regeneration
581 Research. *Trends Neurosci* **41**, 239-242 (2018).

582 5. P. M. Richardson, U. M. Mcguinness, A. J. Aguayo, Axons from Cns Neurons Regenerate into
583 Pns Grafts. *Nature* **284**, 264-265 (1980).

584 6. K. F. So, A. J. Aguayo, Lengthy regrowth of cut axons from ganglion cells after peripheral nerve
585 transplantation into the retina of adult rats. *Brain Res* **328**, 349-354 (1985).

586 7. C. G. Geoffroy, B. Zheng, Myelin-associated inhibitors in axonal growth after CNS injury. *Current*
587 *opinion in neurobiology* **27**, 31-38 (2014).

588 8. J. K. Lee, B. Zheng, Role of myelin-associated inhibitors in axonal repair after spinal cord injury.
589 *Exp Neurol* **235**, 33-42 (2012).

590 9. K. K. Park *et al.*, Promoting axon regeneration in the adult CNS by modulation of the
591 PTEN/mTOR pathway. *Science* **322**, 963-966 (2008).

592 10. P. D. Smith *et al.*, SOCS3 Deletion Promotes Optic Nerve Regeneration In Vivo. *Neuron* **64**, 617-
593 623 (2009).

594 11. D. L. Moore *et al.*, KLF family members regulate intrinsic axon regeneration ability. *Science* **326**,
595 298-301 (2009).

596 12. X. W. Wang *et al.*, Lin28 Signaling Supports Mammalian PNS and CNS Axon Regeneration. *Cell*
597 *Rep* **24**, 2540-2552 e2546 (2018).
598 13. Y. Zhang *et al.*, Elevating Growth Factor Responsiveness and Axon Regeneration by Modulating
599 Presynaptic Inputs. *Neuron* **103**, 39-51 e35 (2019).
600 14. X. Luo *et al.*, Three-dimensional evaluation of retinal ganglion cell axon regeneration and
601 pathfinding in whole mouse tissue after injury. *Exp Neurol* **247**, 653-662 (2013).
602 15. V. Pernet *et al.*, Misguidance and modulation of axonal regeneration by Stat3 and Rho/ROCK
603 signaling in the transparent optic nerve. *Cell Death Dis* **4**, e734 (2013).
604 16. K. Liu *et al.*, PTEN deletion enhances the regenerative ability of adult corticospinal neurons. *Nat*
605 *Neurosci* **13**, 1075-1081 (2010).
606 17. C. G. Geoffroy, B. J. Hilton, W. Tetzlaff, B. Zheng, Evidence for an Age-Dependent Decline in
607 Axon Regeneration in the Adult Mammalian Central Nervous System. *Cell Rep* **15**, 238-246
608 (2016).
609 18. O. Blanquie, F. Bradke, Cytoskeleton dynamics in axon regeneration. *Current opinion in*
610 *neurobiology* **51**, 60-69 (2018).
611 19. E. M. Hur *et al.*, GSK3 controls axon growth via CLASP-mediated regulation of growth cone
612 microtubules. *Genes Dev* **25**, 1968-1981 (2011).
613 20. E. M. Hur, Saijilafu, F. Q. Zhou, Growing the growth cone: remodeling the cytoskeleton to
614 promote axon regeneration. *Trends in Neurosciences* **35**, 164-174 (2012).
615 21. E. M. Hur *et al.*, Engineering neuronal growth cones to promote axon regeneration over inhibitory
616 molecules. *Proc Natl Acad Sci U S A* **108**, 5057-5062 (2011).

617 22. X. Guo, W. D. Snider, B. Chen, GSK3beta regulates AKT-induced central nervous system axon
618 regeneration via an eIF2Bepsilon-dependent, mTORC1-independent pathway. *Elife* **5**, e11903
619 (2016).
620 23. L. Miao *et al.*, mTORC1 is necessary but mTORC2 and GSK3beta are inhibitory for AKT3-
621 induced axon regeneration in the central nervous system. *Elife* **5**, (2016).
622 24. X. Duan *et al.*, Subtype-specific regeneration of retinal ganglion cells following axotomy: effects
623 of osteopontin and mTOR signaling. *Neuron* **85**, 1244-1256 (2015).
624 25. S. Li *et al.*, Promoting axon regeneration in the adult CNS by modulation of the melanopsin/GPCR
625 signaling. *Proc Natl Acad Sci U S A* **113**, 1937-1942 (2016).
626 26. W. Pita-Thomas, M. Mahar, A. Joshi, D. Gan, V. Cavalli, HDAC5 promotes optic nerve
627 regeneration by activating the mTOR pathway. *Exp Neurol* **317**, 271-283 (2019).
628 27. J. H. Lim *et al.*, Neural activity promotes long-distance, target-specific regeneration of adult retinal
629 axons. *Nat Neurosci* **19**, 1073-1084 (2016).
630 28. H. Tsujino *et al.*, Activating transcription factor 3 (ATF3) induction by axotomy in sensory and
631 motoneurons: A novel neuronal marker of nerve injury. *Mol Cell Neurosci* **15**, 170-182 (2000).
632 29. K. Tanabe, I. Bonilla, J. A. Winkles, S. M. Strittmatter, Fibroblast growth factor-inducible-14 is
633 induced in axotomized neurons and promotes neurite outgrowth. *Journal of Neuroscience* **23**,
634 9675-9686 (2003).
635 30. K. J. Christie, C. A. Webber, J. A. Martinez, B. Singh, D. W. Zochodne, PTEN Inhibition to
636 Facilitate Intrinsic Regenerative Outgrowth of Adult Peripheral Axons. *Journal of Neuroscience*
637 **30**, 9306-9315 (2010).
638 31. A. Apara *et al.*, KLF9 and JNK3 Interact to Suppress Axon Regeneration in the Adult CNS.
639 *Journal of Neuroscience* **37**, 9632-9644 (2017).

640 32. Y. Sekine *et al.*, Functional Genome-wide Screen Identifies Pathways Restricting Central Nervous
641 System Axonal Regeneration. *Cell Reports* **23**, 415-428 (2018).
642 33. A. Erturk, F. Hellal, J. Enes, F. Bradke, Disorganized microtubules underlie the formation of
643 retraction bulbs and the failure of axonal regeneration. *J Neurosci* **27**, 9169-9180 (2007).
644 34. F. Hellal *et al.*, Microtubule Stabilization Reduces Scarring and Causes Axon Regeneration After
645 Spinal Cord Injury. *Science* **331**, 928-931 (2011).
646 35. J. Ruschel *et al.*, Axonal regeneration. Systemic administration of epothilone B promotes axon
647 regeneration after spinal cord injury. *Science* **348**, 347-352 (2015).
648 36. V. Sengottuvel, M. Leibinger, M. Pfreimer, A. Andreadaki, D. Fischer, Taxol facilitates axon
649 regeneration in the mature CNS. *J Neurosci* **31**, 2688-2699 (2011).
650 37. F. Sun *et al.*, Sustained axon regeneration induced by co-deletion of PTEN and SOCS3. *Nature*
651 **480**, 372-375 (2011).
652 38. T. Kurimoto *et al.*, Long-distance axon regeneration in the mature optic nerve: contributions of
653 oncomodulin, cAMP, and pten gene deletion. *The Journal of neuroscience : the official journal of*
654 *the Society for Neuroscience* **30**, 15654-15663 (2010).
655 39. S. de Lima *et al.*, Full-length axon regeneration in the adult mouse optic nerve and partial recovery
656 of simple visual behaviors. *Proc Natl Acad Sci U S A* **109**, 9149-9154 (2012).
657 40. B. H. Varkuti *et al.*, A highly soluble, non-phototoxic, non-fluorescent blebbistatin derivative. *Sci*
658 *Rep* **6**, 26141 (2016).
659 41. A. Erturk *et al.*, Three-dimensional imaging of solvent-cleared organs using 3DISCO. *Nat Protoc*
660 **7**, 1983-1995 (2012).
661 42. D. Kim, B. Langmead, S. L. Salzberg, HISAT: a fast spliced aligner with low memory
662 requirements. *Nat Methods* **12**, 357-360 (2015).

663 43. M. Pertea *et al.*, StringTie enables improved reconstruction of a transcriptome from RNA-seq
664 reads. *Nat Biotechnol* **33**, 290-295 (2015).
665 44. M. Pertea, D. Kim, G. M. Pertea, J. T. Leek, S. L. Salzberg, Transcript-level expression analysis
666 of RNA-seq experiments with HISAT, StringTie and Ballgown. *Nat Protoc* **11**, 1650-1667 (2016).
667 45. A. Mortazavi, B. A. Williams, K. McCue, L. Schaeffer, B. Wold, Mapping and quantifying
668 mammalian transcriptomes by RNA-Seq. *Nat Methods* **5**, 621-628 (2008).
669 46. M. D. Robinson, D. J. McCarthy, G. K. Smyth, edgeR: a Bioconductor package for differential
670 expression analysis of digital gene expression data. *Bioinformatics* **26**, 139-140 (2010).
671 47. Y. Benjamini, Y. Hochberg, Controlling the False Discovery Rate - a Practical and Powerful
672 Approach to Multiple Testing. *J R Stat Soc B* **57**, 289-300 (1995).
673 48. Y. Benjamini, D. Yekutieli, The control of the false discovery rate in multiple testing under
674 dependency. *Ann Stat* **29**, 1165-1188 (2001).
675 49. D. W. Huang, B. T. Sherman, R. A. Lempicki, Systematic and integrative analysis of large gene
676 lists using DAVID bioinformatics resources. *Nature Protocols* **4**, 44-57 (2009).
677 50. D. W. Huang, B. T. Sherman, R. A. Lempicki, Bioinformatics enrichment tools: paths toward the
678 comprehensive functional analysis of large gene lists. *Nucleic Acids Research* **37**, 1-13 (2009).
679

680 **Acknowledgements:** We appreciate Dr. Michele Pucak's help in confocal imaging experiments and
681 analyses. **Funding:** The study was supported by grants (to F.Q.Z.) from NIH (R01NS064288,
682 R01NS085176, R01GM111514, R01EY027347), the Craig H. Neilsen Foundation (259450), and
683 the BrightFocus Foundation (G2017037). Saijilafu was supported by the grants from the National Natural
684 Science Foundation of China (81571189, 81772353), the National Key Research and Development
685 Program (2016YFC1100203), and Innovation and Entrepreneurship Program of Jiangsu Province. **Author**

686 **contributions:** X.-W.W., S.-G.Y., S., and F.-Q.Z. conceived the study and designed the project; X.-W.W.
687 and S.-G.Y. performed most of the experiments; C.Z. performed and analyzed the immunostaining
688 experiments; Y.Z. analyzed optic nerve regeneration; C.Z. and Y.Z. analyzed the axon morphologies and
689 trajectories; J.-J.M. performed the sensory neuron RNA-seq experiment; Y.-L.W. and G.-L.M. helped
690 with the optic nerve regeneration experiments; B.-B.Y., and A.R.K. helped with the data analyses; X.-
691 W.W. and F.-Q.Z. wrote the manuscript with contribution from all authors. **Competing interests:** The
692 authors declare no competing interests. **Data and material availability:** The data that support the findings
693 of this study are available from the authors upon request. RNA-seq raw data will be deposited and
694 accession code will be available before publication.

Figure 1

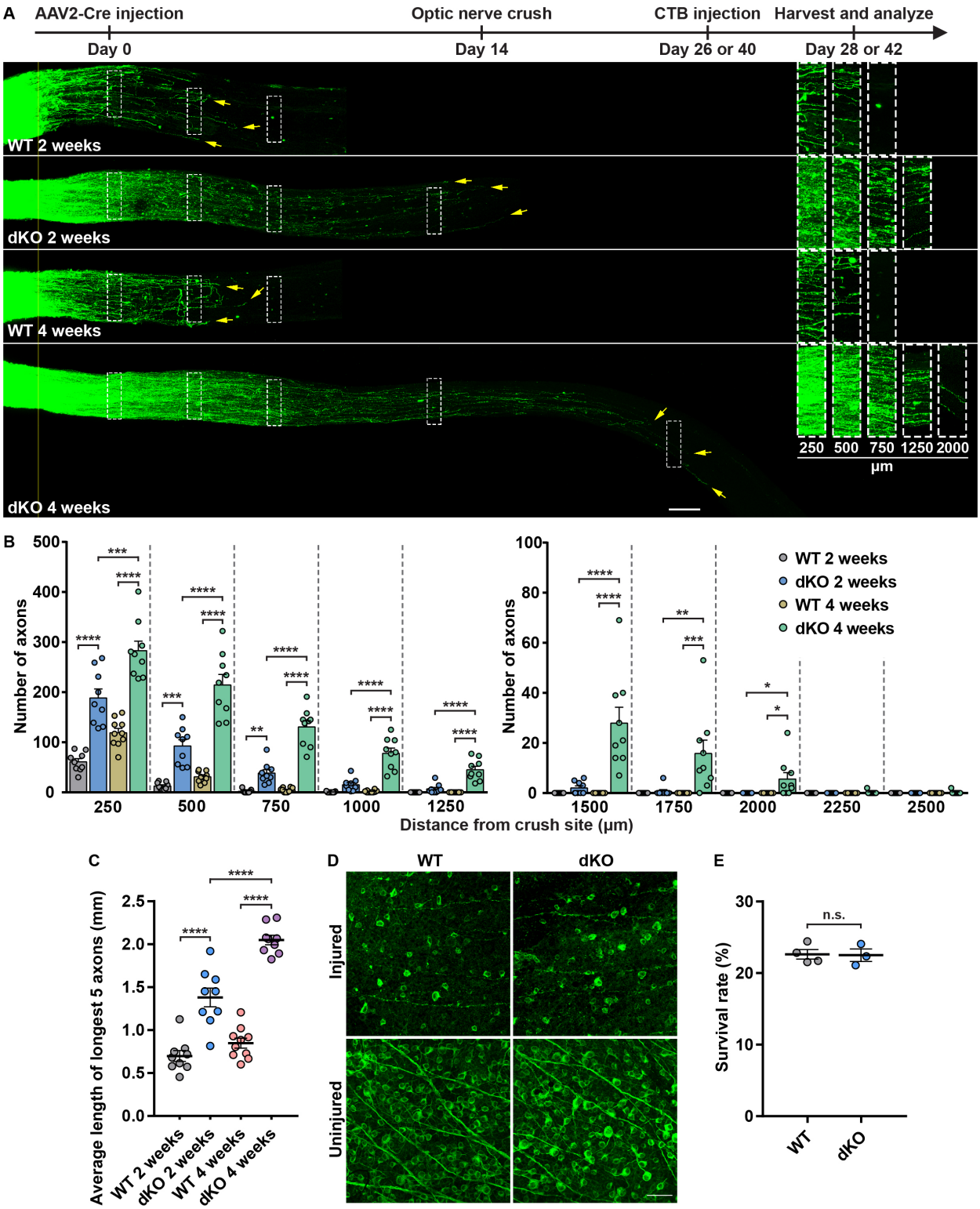
A
AAV2-Cre injection
Optic nerve crush
CTB injection
Harvest and analyze
Day 0
Day 14
Day 26 or 40
Day 28 or 42
WT 2 weeks
dKO 2 weeks
WT 4 weeks
dKO 4 weeks
250 500 750 1250 2000
µm
B
Number of axons
Distance from crush site (µm)
WT 2 weeks
dKO 2 weeks
WT 4 weeks
dKO 4 weeks
C
Average length of longest 5 axons (mm)
WT 2 weeks
dKO 2 weeks
WT 4 weeks
dKO 4 weeks
D
WT
dKO
Injured
Uninjured
E
Survival rate (%)
n.s.
WT
dKO

697 **Fig. 1. Deletion of myosin IIA/B in RGCs induced robust and sustained optic nerve regeneration.**

698

699 (A) Top: experimental timeline. Bottom: representative images of optic nerves showing that deletion of
700 myosin IIA/B in RGCs produced robust and persistent axon regeneration 2 and 4 weeks after optic nerve
701 crush. The columns on the right display magnified images of the areas in white dashed boxes on the left,
702 showing axons at 250, 500, 750, 1250 and 2000 μm distal to the crush sites. The yellow line indicates the
703 crush sites. Yellow arrows indicate the top 3 longest axons of each nerve. Scale bar, 100 μm (50 μm for
704 the magnified images).

705

706 (B) Quantification of optic nerve regeneration in (A) (one-way ANOVA followed by Tukey's multiple
707 comparisons test, $P < 0.0001$ at 250, 500, 750, 1000, 1250 and 1500 μm, $P = 0.0002$, 0.0071, 0.3875 and
708 0.3875 at 1750, 2000, 2250 and 2500 μm, respectively; n = 10 mice in 4-week WT group, n = 9 mice in
709 other groups).

710

711 (C) Quantification of the average length of the top 5 longest axons of each nerve in (A) (one-way ANOVA
712 followed by Tukey's multiple comparisons test, $P < 0.0001$; n = 10 mice in 4-week WT group, n = 9 mice
713 in other groups).

714

715 (D) Representative images of flat-mounted retinas showing that deletion of myosin IIA/B had no effect
716 on RGC survival rate 2 weeks after optic nerve crush. Flat-mounted retinas were stained with anti-tubulin
717 β3 antibody (Tuj1, green). Scale bar, 50 μm.

718

719 (E) Quantification of RGC survival rate in (D) (unpaired t test, $P = 0.9092$, n = 4 and 3 mice in WT and

720 dKO groups, respectively, 7-8 fields were analyzed for each retina).

721

722 Data are represented as mean ± SEM. n.s., not significant, *$P < 0.05$, **$P < 0.01$, ***$P < 0.001$, ****$P <$

723 0.0001. WT, wild type; dKO, double knockout of myosin IIA/B.

Figure 2

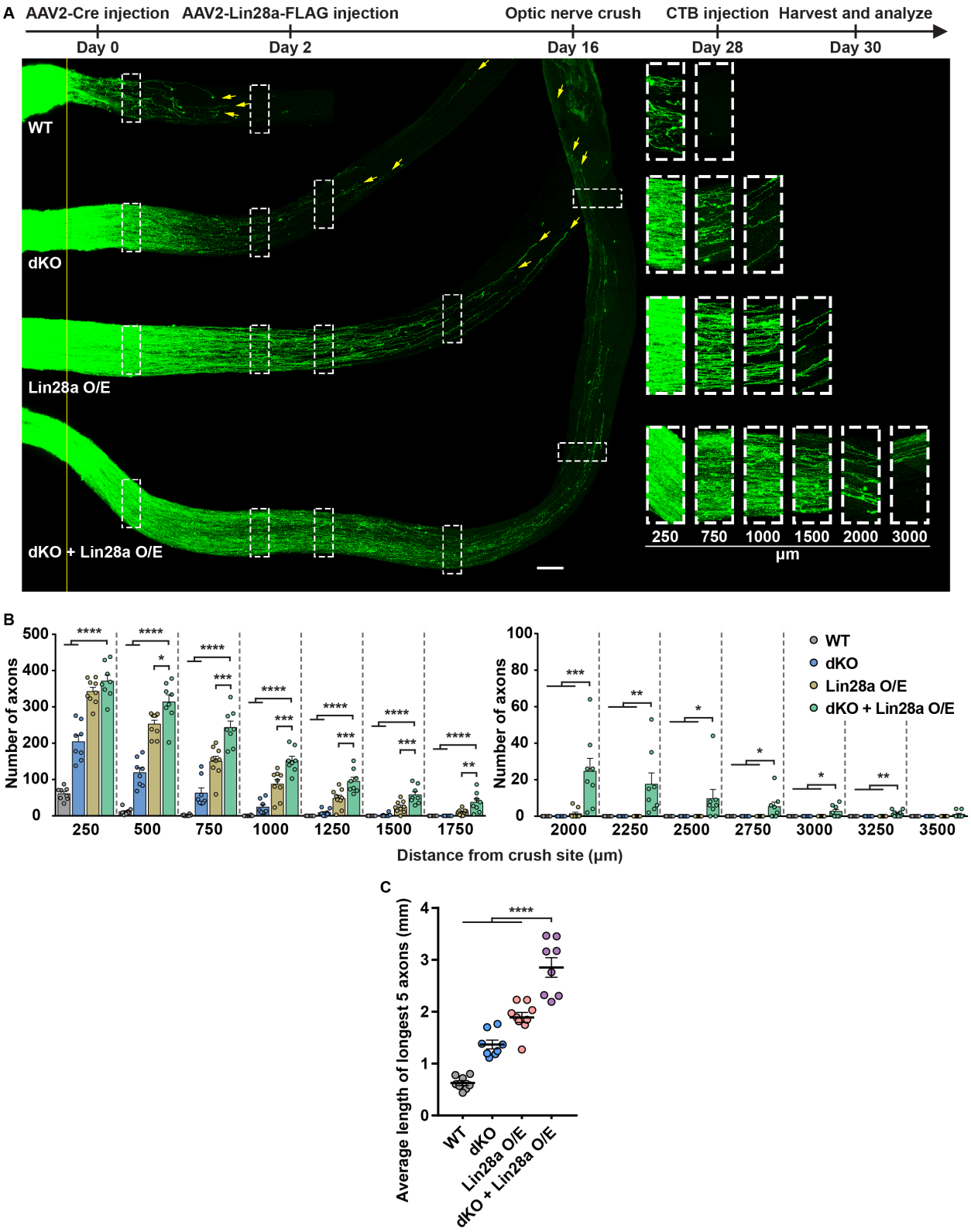
A
AAV2-Cre injection
AAV2-Lin28a-FLAG injection
Optic nerve crush
CTB injection
Harvest and analyze
Day 0
Day 2
Day 16
Day 28
Day 30
WT
dKO
Lin28a O/E
dKO + Lin28a O/E
250
750
1000
1500
2000
3000
µm
B
Number of axons
Distance from crush site (µm)
WT
dKO
Lin28a O/E
dKO + Lin28a O/E
C
Average length of longest 5 axons (mm)
WT
dKO
Lin28a O/E
dKO + Lin28a O/E

726 **Fig. 2. Myosin IIA/B deletion and Lin28a overexpression had synergistic effect on optic nerve**
727 **regeneration.**
728
729 (A) Top: experimental timeline. Bottom: representative images of optic nerves showing that combining
730 myosin IIA/B deletion with Lin28a overexpression in RGCs produced much stronger axon regeneration
731 2 weeks after the optic nerve crush. The columns on the right display magnified images of the areas in
732 white dashed boxes on the left, showing axons at 250, 750, 1000, 1500, 2000 and 3000 μm distal to the
733 crush sites. The yellow line indicates the crush sites. Yellow arrows indicate the top 3 longest axons of
734 each nerve. Scale bar, 100 μm (50 μm for the magnified images).
735
736 (B) Quantification of optic nerve regeneration in (A) (one-way ANOVA followed by Tukey's multiple
737 comparisons test, $P < 0.0001$ at 250, 500, 750, 1000, 1250, 1500, 1750 and 2000 μm, $P = 0.0004$, 0.0206,
738 0.0092, 0.0042, 0.0026, 0.0844 at 2250, 2500, 2750, 3000, 3250 and 3500 μm, respectively; n = 9 mice
739 in Lin28a O/E group, n = 8 mice in other groups).
740
741 (C) Quantification of the average length of the top 5 longest axons of each nerve in (A) (one-way ANOVA
742 followed by Tukey's multiple comparisons test, $P < 0.0001$; n = 9 mice in Lin28a O/E group, n = 8 mice
743 in other groups).
744
745 Data are represented as mean ± SEM. n.s., not significant, *$P < 0.05$, **$P < 0.01$, ***$P < 0.001$, ****$P <$
746 0.0001. WT, wild type; dKO, double knockout of myosin IIA/B; O/E, overexpression.

Figure 3

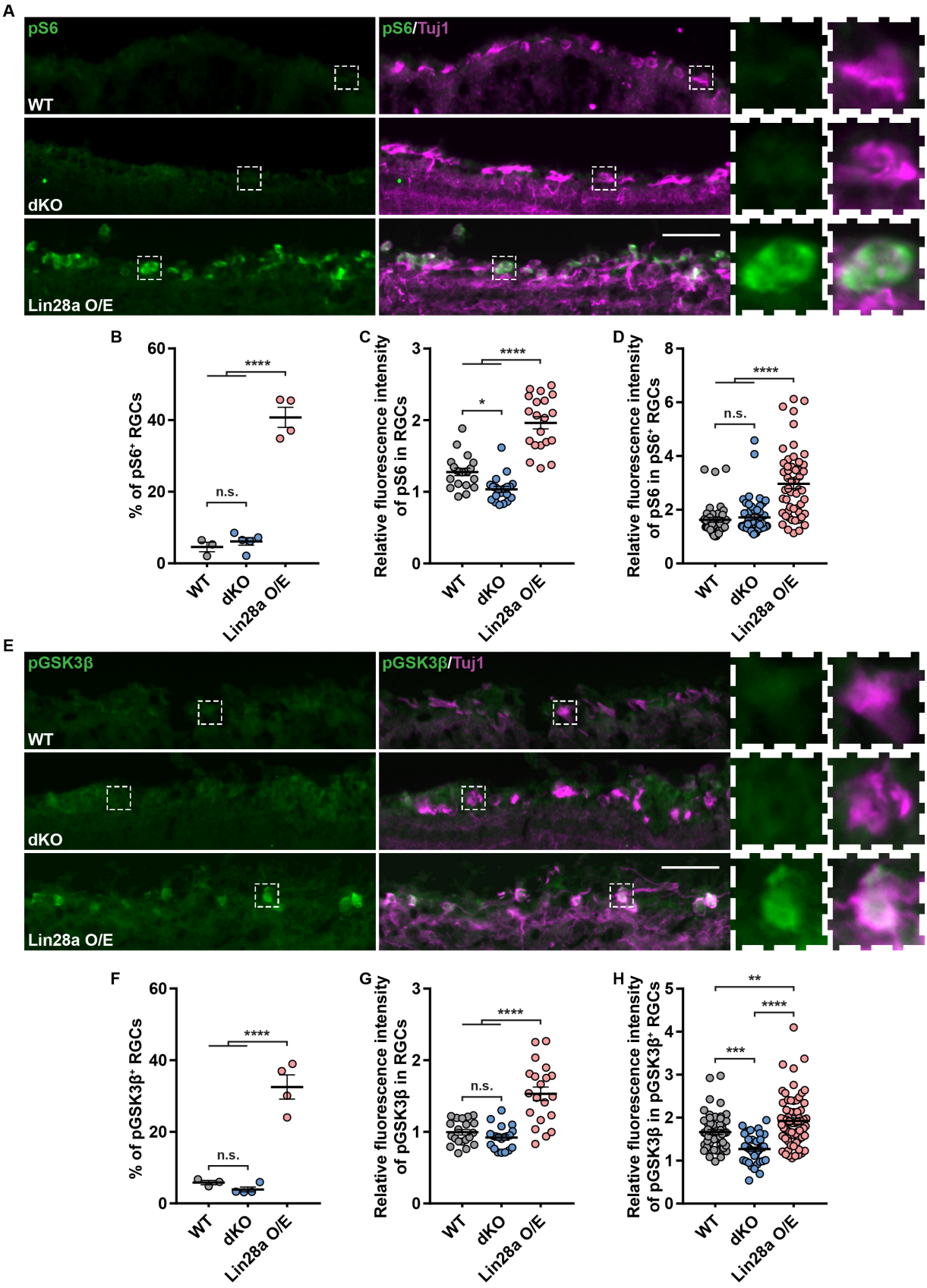
A
pS6
pS6/Tuj1
WT
dKO
Lin28a O/E
B
% of pS6⁺ RGCs
****
n.s.
C
Relative fluorescence intensity of pS6 in RGCs
****
*
D
Relative fluorescence intensity of pS6 in pS6⁺ RGCs
****
n.s.
E
pGSK3β
pGSK3β/Tuj1
WT
dKO
Lin28a O/E
F
% of pGSK3β⁺ RGCs
****
n.s.
G
Relative fluorescence intensity of pGSK3β in RGCs
****
n.s.
H
Relative fluorescence intensity of pGSK3β in pGSK3β⁺ RGCs
**
****
***
WT
dKO
Lin28a O/E

747

748 **Fig. 3. Myosin IIA/B deletion-induced optic nerve regeneration was independent of mTOR or**
749 **GSK3β pathway.**
750
751 (A) Representative images of retinal sections showing that the deletion of myosin IIA/B did not activate
752 mTOR (marked by pS6) in RGCs, whereas Lin28a overexpression markedly activated mTOR in RGCs 2
753 weeks after optic nerve crush. The two columns on the right display magnified images of the RGCs marked
754 in white dashed boxes on the left. Retinal sections were stained with anti-pS6 (green) and anti-tubulin β3
755 (magenta) antibodies. Scale bar, 50 μm (12.5 μm for the magnified images).
756
757 (B) Quantification of the percentage of $pS6^+$ RGCs in (A) (one-way ANOVA followed by Tukey's
758 multiple comparisons, $P < 0.0001$, n = 3 mice in WT group, n = 5 mice in dKO group, n = 4 mice in
759 Lin28a O/E group, at least 363 RGCs from at least 7 non-adjacent retinal sections were analyzed for each
760 mouse).
761
762 (C) Quantification of average fluorescence intensity of pS6 in all RGCs (one-way ANOVA followed by
763 Tukey's multiple comparisons, $P < 0.0001$, n = 20 retinal sections with identical imaging configurations
764 from at least 2 mice were analyzed for each group).
765
766 (D) Quantification of average fluorescence intensity of pS6 in $pS6^+$ RGCs (one-way ANOVA followed
767 by Tukey's multiple comparisons, $P < 0.0001$, n = 42, 49 and 53 RGCs with identical imaging
768 configurations from at least 2 mice were analyzed for WT, dKO and Lin28a O/E groups, respectively).
769

770 (E) Representative images of retinal sections showing that the deletion of myosin IIA/B did not inactivate
771 GSK3β (marked by pGSK3β) in RGCs, whereas Lin28a overexpression markedly inactivated GSK3β in
772 RGCs 2 weeks after optic nerve crush. The right two columns display magnified images of the RGCs
773 marked in white dashed boxes on the left. Retinal sections were stained with anti-pGSK3β (green) and
774 anti-tubulin β3 (magenta) antibodies. Scale bar, 50 μm (12.5 μm for the magnified images).
775
776 (F) Quantification of the percentage of pGSK3β^{+} RGCs in (E) (one-way ANOVA followed by Tukey's
777 multiple comparisons, $P < 0.0001$, n = 3 mice in WT group, n = 4 mice in other groups, at least 434 RGCs
778 from at least 7 non-adjacent retinal sections were analyzed for each mouse).
779
780 (G) Quantification of average fluorescence intensity of pGSK3β in all RGCs (one-way ANOVA followed
781 by Tukey's multiple comparisons, $P < 0.0001$, n = 20 retinal sections with identical imaging
782 configurations from at least 2 mice were analyzed for each group).
783
784 (H) Quantification of average fluorescence intensity of pGSK3β in pGSK3β^{+} RGCs (one-way ANOVA
785 followed by Tukey's multiple comparisons, $P < 0.0001$, n = 54, 40 and 65 RGCs with identical imaging
786 configurations from at least 2 mice were analyzed for WT, dKO and Lin28a O/E groups, respectively).
787
788 Data are represented as mean ± SEM. n.s., not significant, *$P < 0.05$, **$P < 0.01$, ***$P < 0.001$, ****$P <$
789 0.0001. WT, wild type; dKO, double knockout of myosin IIA/B; O/E, overexpression.

Figure 4

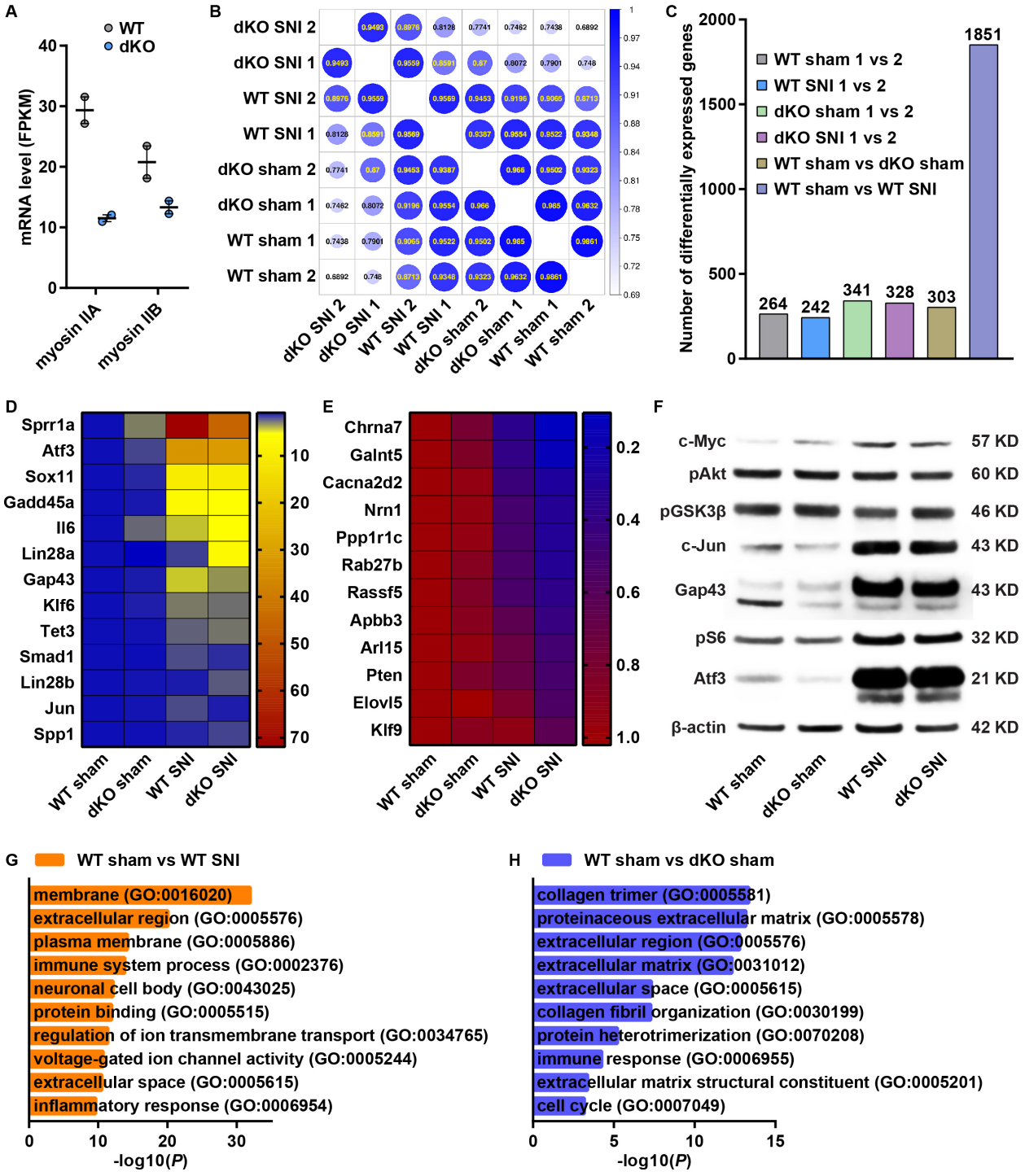
A
WT
dKO
mRNA level (FPKM)
myosin IIA
myosin IIB
B
dKO SNI 2
dKO SNI 1
WT SNI 2
WT SNI 1
dKO sham 2
dKO sham 1
WT sham 1
WT sham 2
C
Number of differentially expressed genes
WT sham 1 vs 2
WT SNI 1 vs 2
dKO sham 1 vs 2
dKO SNI 1 vs 2
WT sham vs dKO sham
WT sham vs WT SNI
264
242
341
328
303
1851
D
Sprr1a
Atf3
Sox11
Gadd45a
Il6
Lin28a
Gap43
Klf6
Tet3
Smad1
Lin28b
Jun
Spp1
WT sham
dKO sham
WT SNI
dKO SNI
E
Chrna7
Galnt5
Cacna2d2
Nrn1
Ppp1r1c
Rab27b
Rassf5
Apbb3
Arl15
Pten
Elovl5
Klf9
F
c-Myc 57 KD
pAkt 60 KD
pGSK3β 46 KD
c-Jun 43 KD
Gap43 43 KD
pS6 32 KD
Atf3 21 KD
β-actin 42 KD
G
WT sham vs WT SNI
membrane (GO:0016020)
extracellular region (GO:0005576)
plasma membrane (GO:0005886)
immune system process (GO:0002376)
neuronal cell body (GO:0043025)
protein binding (GO:0005515)
regulation of ion transmembrane transport (GO:0034765)
voltage-gated ion channel activity (GO:0005244)
extracellular space (GO:0005615)
inflammatory response (GO:0006954)
-log10(P)
H
WT sham vs dKO sham
collagen trimer (GO:0005581)
proteinaceous extracellular matrix (GO:0005578)
extracellular region (GO:0005576)
extracellular matrix (GO:0031012)
extracellular space (GO:0005615)
collagen fibril organization (GO:0030199)
protein heterotrimerization (GO:0070208)
immune response (GO:0006955)
extracellular matrix structural constituent (GO:0005201)
cell cycle (GO:0007049)
-log10(P)

794 **Fig. 4. Conditional knockout of myosin IIA/B in sensory neurons did not significantly affect known**
795 **regeneration associated genes and pathways**
796
797 (A) Decreased mRNA levels of myosin IIA/B in L4/5 DRGs of *Advillin-Cre: myosin IIA/B*$^{f/f}$ mice (n = 2
798 mice in each group, data are represented as mean ± SEM).
799
800 (B) Pearson correlation heatmap showing the high degree of similarity in gene transcription between wild
801 type and myosin IIA/B deleted neurons under the same condition (sham or SNI).
802
803 (C) Number of differentially expressed genes between replicates or conditions showing that myosin IIA/B
804 deletion did not significantly change gene expression in neurons.
805
806 (D, E) Expression heatmap of genes known to be upregulated (D) or downregulated (E) following SNI.
807 Results showed that myosin IIA/B deletion did not affect the transcription of these genes in neurons.
808
809 (F) Representative western blot results showing that neuron specific myosin IIA/B conditional knockout
810 did not affect classic regeneration associated genes or pathways (n = 3 independent experiments).
811
812 (G, H) Gene ontology analyses of differentially expressed genes between uninjured (sham) and injured
813 (SNI) condition in wild type neurons (G), and between wild type neurons and myosin IIA/B deleted
814 neurons under uninjured (sham) condition (H).
815
816 WT, wild type. dKO, double knockout of myosin IIA/B. SNI, sciatic nerve injury.

Figure 5

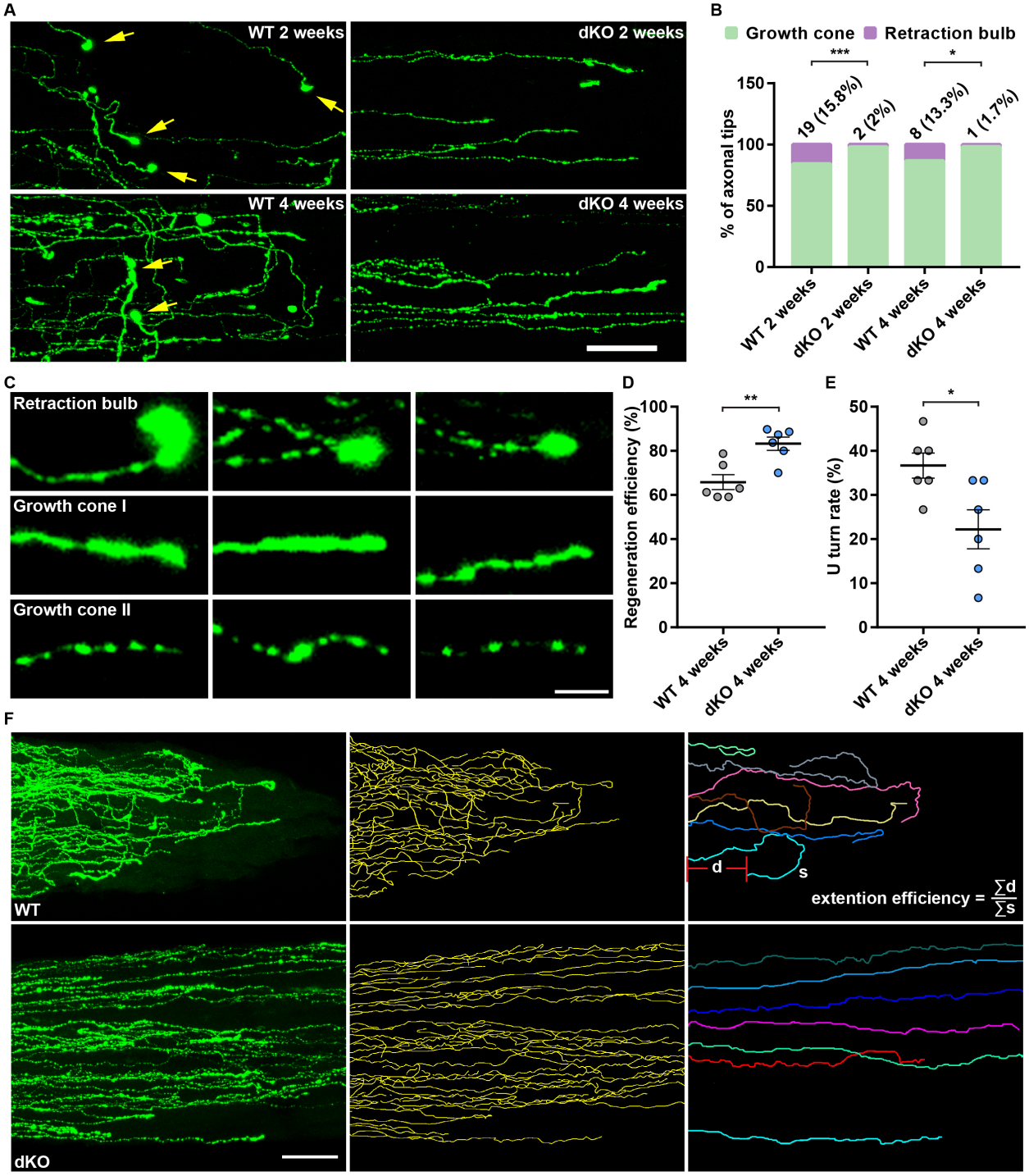

817

818

819

820

821 **Fig. 5. Myosin IIA/B deletion modified cytoskeletal dynamics to promote axon regeneration.**

822

823 (A) Representative images of optic nerves showing that the deletion of myosin IIA/B in RGCs abolished
824 the formation of retraction bulbs in optic nerves 2 and 4 weeks after optic nerve crush. Yellow arrows
825 indicate retraction bulbs. Scale bar, 50 μm.

826

827 (B) Quantification of retraction bulbs in (A) (Fisher's exact test, $P = 0.0004$ and 0.0322 for 2 weeks and
828 4 weeks after optic nerve crush, respectively; n = 120 and 100 axonal tips from 12 nerves in 2-week WT
829 and 10 nerves in dKO groups, respectively, n = 60 axonal tips from 6 nerves in each 4-week group).

830

831 (C) Representative images of retraction bulbs and growth cones found in different optic nerves. Scale bar,
832 5 μm.

833

834 (D) Quantification of axon extension efficiency in (F) and Fig. S5 (unpaired t test, $P = 0.0032$, n = 6 mice
835 in each group, at least 35 axons were analyzed for each mouse).

836

837 (E) Quantification of U-turn rate in Fig. S6 (unpaired t test, $P = 0.0210$, n = 6 mice in each group, top 15
838 longest axons were analyzed for each mouse).

839

840 (F) Left: representative images of optic nerves showing that the deletion of myosin IIA/B in RGCs
841 improved axon extension efficiency 4 weeks after optic nerve crush. Middle: sketches of all axon traces
842 in the left column. Right: detailed trajectories of a few axons (each color represents a single axon) in the

843 left column. As illustrated, the extension efficiency of each nerve was calculated by dividing the summed
844 displacement by the summed length of all traced axons. Scale bar, 50 μm.
845
846 Data are represented as mean ± SEM. *$P < 0.05$, **$P < 0.01$, ***$P < 0.001$. WT, wild type; dKO, double
847 knockout of myosin IIA/B.
848
849
850
851

Figure 6

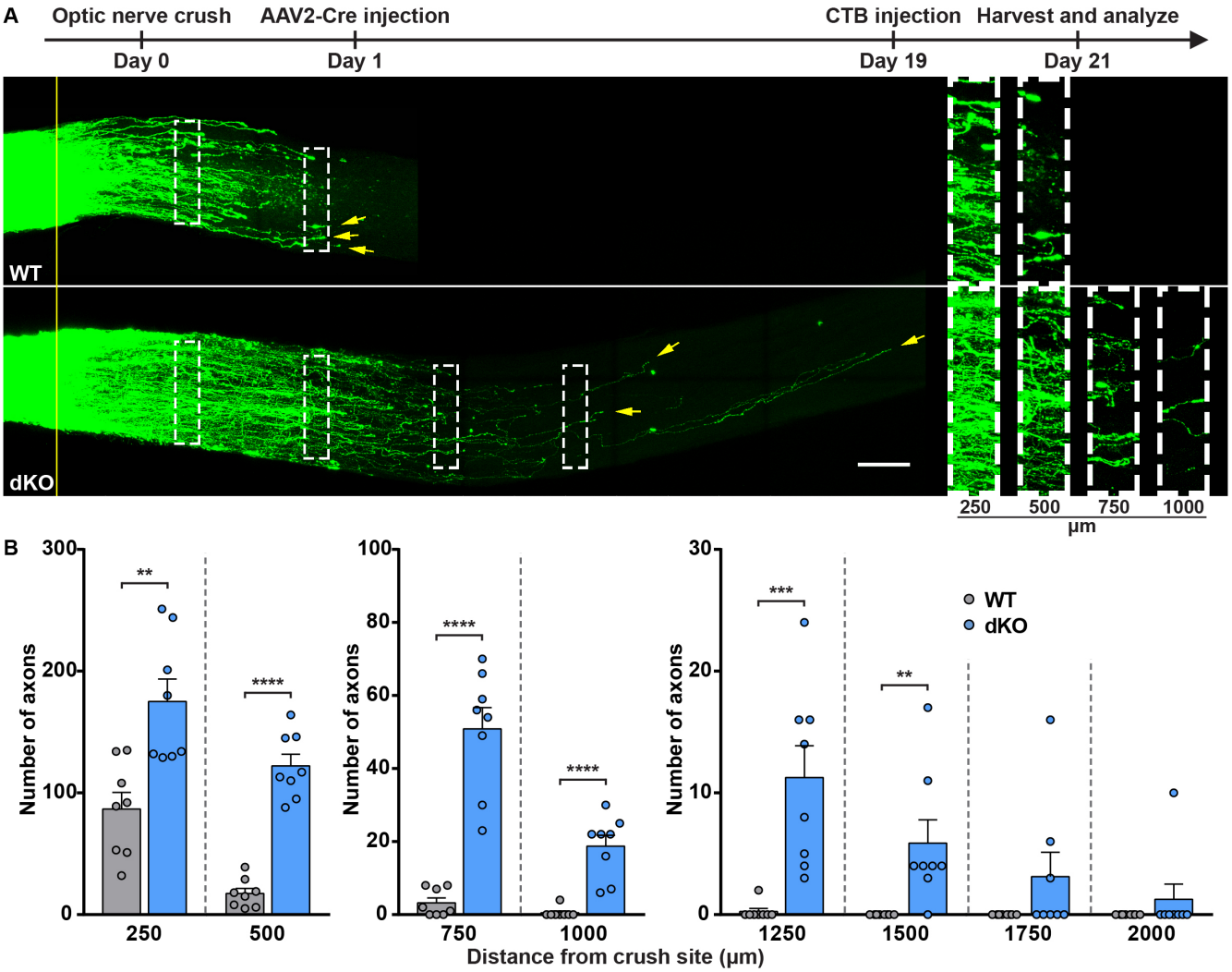

852

853 **Fig. 6. Post-injury deletion of myosin IIA/B could also induce optic nerve regeneration.**

854

855 (A) Top: experimental timeline. Bottom: representative images of optic nerves showing that post-injury
856 deletion of myosin IIA/B in RGCs induced axon regeneration 3 weeks after optic nerve crush. The
857 columns on the right display magnified images of the areas in white dashed boxes on the left, showing
858 axons at 250, 500, 750 and 1000 μm distal to the crush sites. The yellow line indicates the crush sites.
859 Yellow arrows indicate the top 3 longest axons of each nerve. Scale bar, 100 μm (50 μm for the magnified
860 images).

861

862 (B) Quantification of optic nerve regeneration in (A) (unpaired t test, $P = 0.0017$ at 250 μm, $P < 0.0001$

863 at 500, 750 and 1000 μm, $P = 0.0009$, 0.0085, 0.1396 and 0.3343 at 1250, 1500, 1750 and 2000 μm,

864 respectively; n = 8 mice in each group).

865

866

867

868

869

870

871

Figure S1

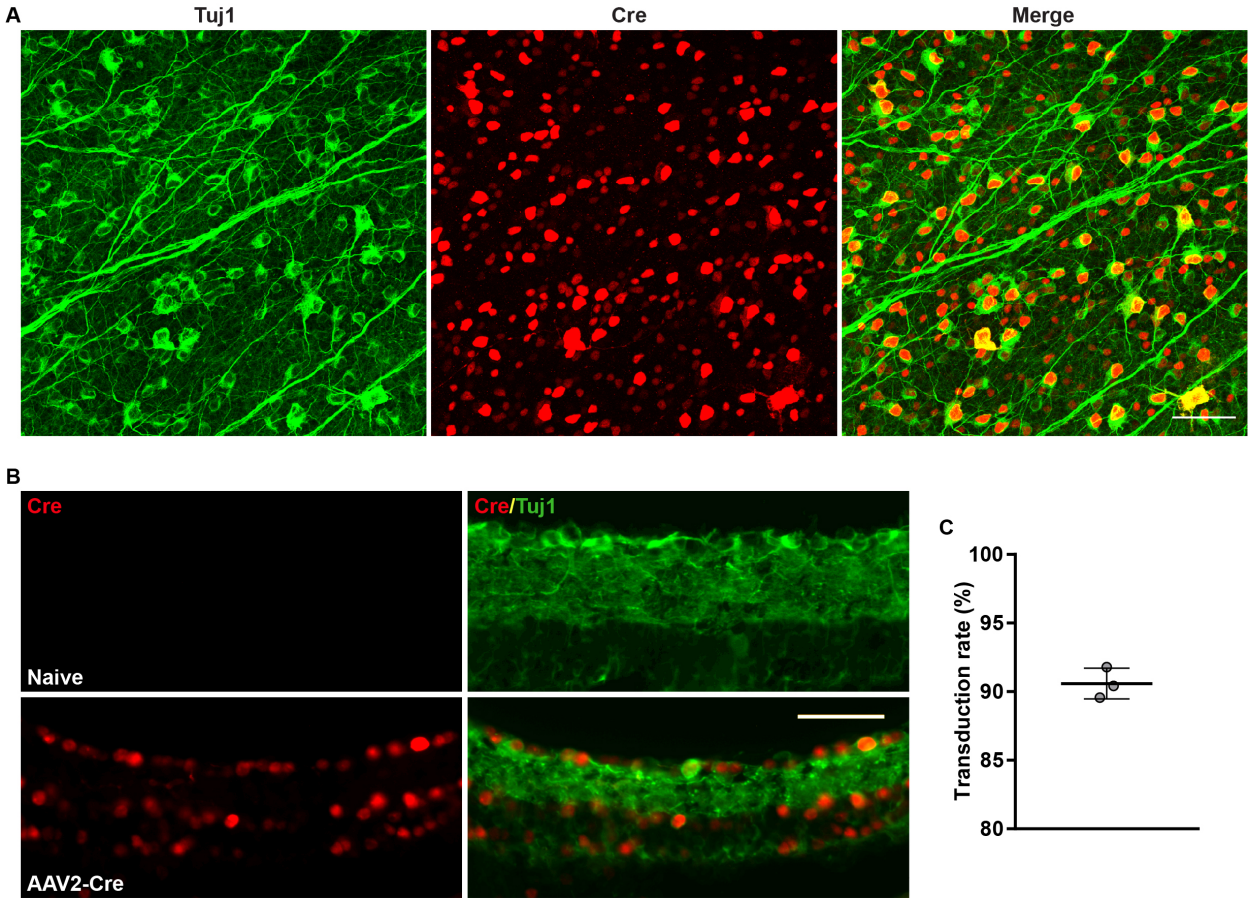

872

873 **Fig. S1. Transduction rate of AAV2-Cre. Related to Fig. 1.**

874

875 (A) Representative images of flat-mounted retinas showing the high transduction rate of AAV2-Cre in
876 RGCs. Flat-mounted retinas were stained with anti-tubulin β3 (Tuj1, green) and anti-Cre recombinase
877 (red) antibodies. Scale bar, 50 μm.

878

879 (B) Representative images of retinal sections verifying the specificity of the anti-Cre antibody and the
880 high transduction rate of AAV2-Cre in RGCs. Retinal sections were stained with anti-tubulin β3 (Tuj1,
881 green) and anti-Cre (red) antibodies. Scale bar, 50 μm.

882

883 (C) Quantification of the transduction rate of AAV2-Cre in RGCs in (A). The average transduction rate

884 was 90.59 ± 1.114% (n = 3 mice, 5-8 fields were analyzed for each mouse, data are represented as mean

885 ± SD).

886

Figure S2

A

B

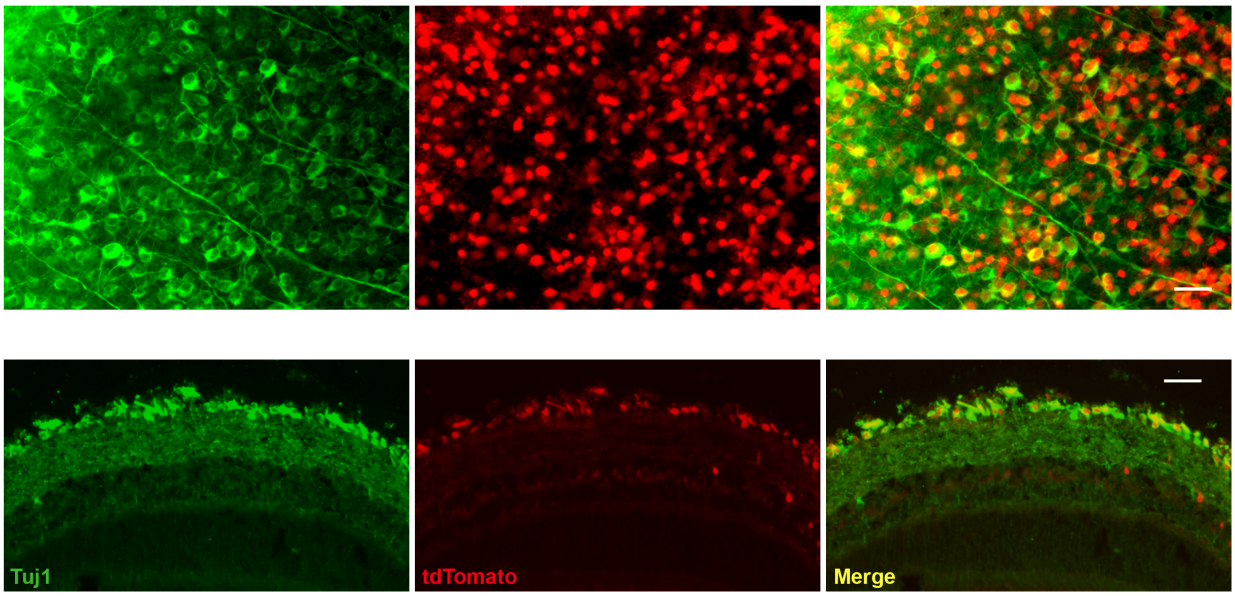

887

888 **Fig. S2. Verification of the Cre-mediated gene recombination. Related to Fig. 1.**

889

890 (A, B) Representative images of flat-mounted retinas (A) and retinal sections (B) showing the expression

891 of tdTomato in RGCs of tdTomato reporter mice, indicating successful Cre-mediated gene recombination

892 2 weeks after intravitreal AAV2-Cre injection. Flat-mounted retinas and retinal sections were stained with

893 anti-tubulin β3 (Tuj1, green). Scale bar, 50 μm.

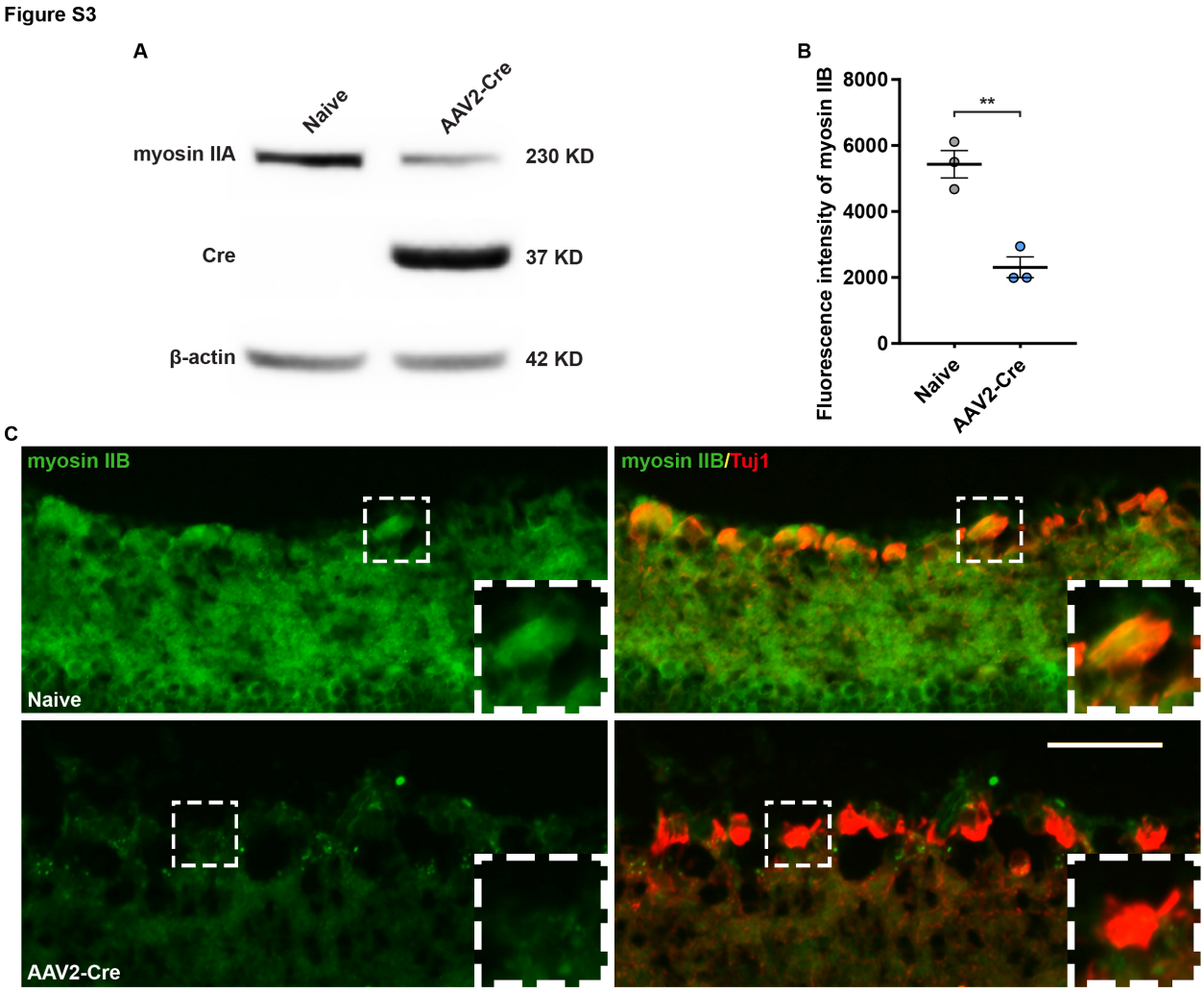

Fig. S3. Verification of myosin IIA/B deletion. Related to Fig. 1.

(A) Western blot result showing the decreased protein level of myosin IIA in retina of a *myosin IIA/B*$^{f/f}$ mouse 2 weeks after intravitreal AAV2-Cre injection.

(B) Quantification of average fluorescence intensity of myosin IIB in (C) (paired t test, $P = 0.0057$, n = 3 mice, data are represented as mean ± SEM, $^{**}P < 0.01$, all images were taken with identical configurations).

904 (C) Representative images of retinal sections from the naïve (top) or the AAV2-Cre injected retina (bottom)
905 of a *myosin IIA/B*$^{f/f}$ mouse showing the successful deletion of myosin IIB in RGCs 2 weeks after
906 intravitreal AAV2-Cre injection. The insets display magnified images of the RGCs marked in white
907 dashed boxes. Retinal sections were stained with anti-tubulin β3 (Tuj1, red) and anti-myosin IIB (green)
908 antibodies. Scale bar, 50 μm (25 μm for the magnified images).
909

Figure S4

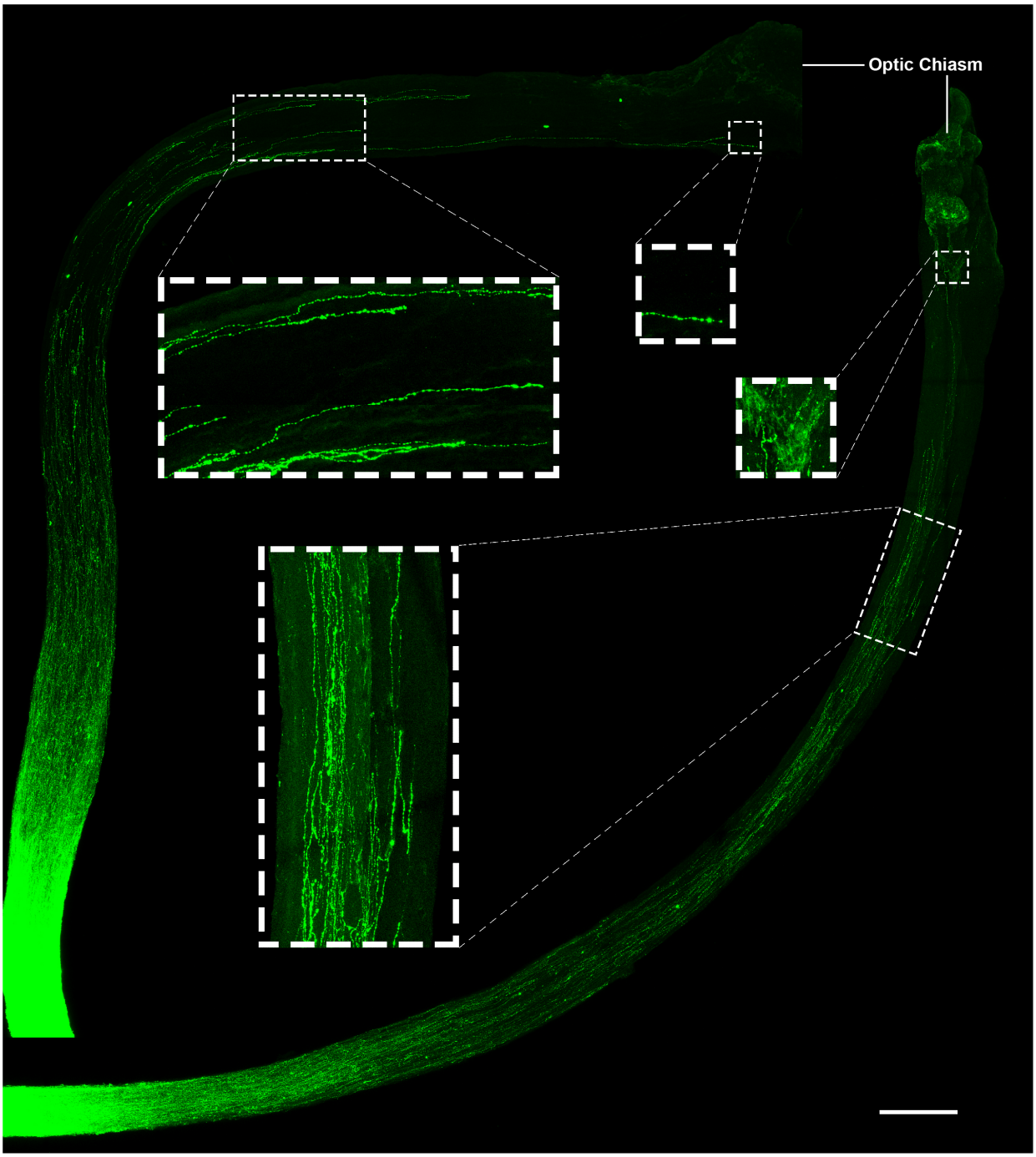

910

911

912

913

914 **Fig. S4. Combination of myosin IIA/B deletion and Lin28a overexpression greatly enhanced optic**

915 **nerve regeneration up to the optic chiasm. Related to Fig. 2.**

916

917 Images of two optic nerves in the combinatory treatment group with longest axons reaching optic chiasm.

918 Magnified images show detailed morphologies of axons in white dashed boxes. Scale bar, 200 μm (66.7

919 μm for the magnified images).

920

Figure S5

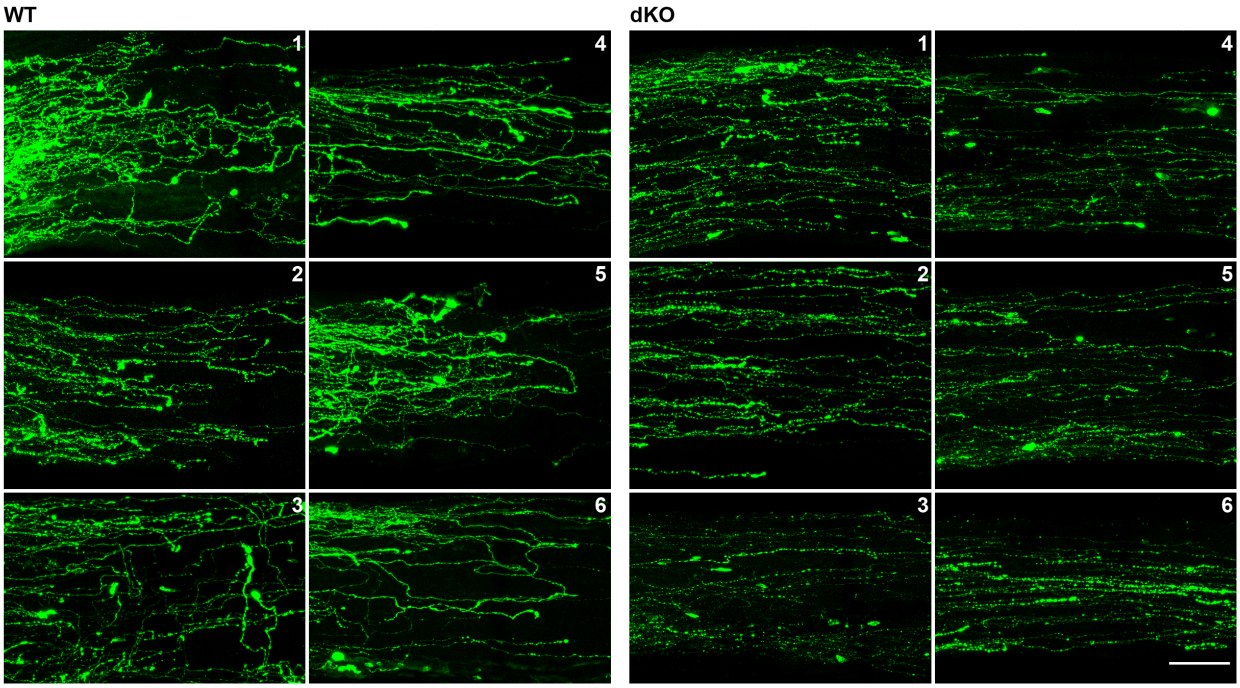

921

922 **Fig. S5. Deletion of myosin IIA/B in RGCs improved axon extension efficiency. Related to Fig. 5.**

923

924 Images of the regions used for the quantification of axon extension efficiency (one region from each optic

925 nerve). Scale bar, 50 μm. WT, wild type; dKO, double knockout of myosin IIA/B.

926

Figure S6

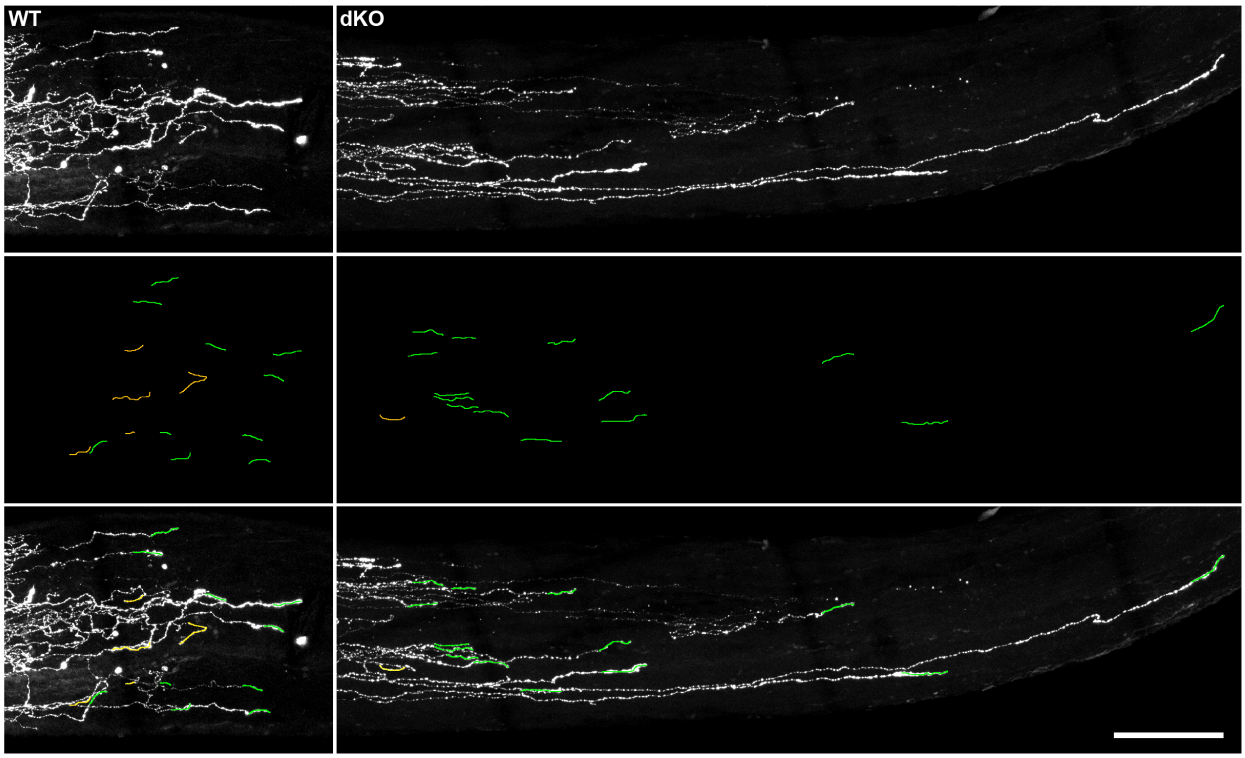

Fig. S6. Deletion of myosin IIA/B reduced U-turn rate. Related to Fig. 5.

Top: representative images of the leading-edge area of optic nerves showing that myosin IIA/B deletion reduced U-turn rate. Middle: axon trajectories near axonal tips, U-turns are labeled in yellow. Bottom: overlay of top and middle rows. Scale bar, 50 μm. WT, wild type; dKO, double knockout of myosin IIA/B.

Movie S1. A 3D animation of regenerating axons in an optic nerve.